JOURNAL OF GEOPHYSICAL RESEARCH, VOL. 114, B00A12, doi:10.1029/2008JB006046, 2009

Northern Cascadia episodic tremor and slip: A decade of tremor observations from 1997 to 2007

Honn Kao,[1] Shao-Ju Shan,[1] Herb Dragert,[1] and Garry Rogers[1]

Received 29 August 2008; revised 26 June 2009; accepted 22 July 2009; published 21 November 2009.

[1] We analyze continuous seismic and GPS records collected in the last decade (1997–2007) to establish the most comprehensive observational basis for northern Cascadia episodic tremor and slip (ETS) events. A simple "ETS scale" system, using a combination of a letter and a digit, is proposed to quantitatively characterize the spatial and temporal dimensions of ETS events. Clear correlation between GPS and tremor signals is observed for all A/B class episodes, but the GPS signature is less obvious for minor ones. Regular ETS recurrence can be established only for A/B class episodes in southern Vancouver Island. Halting and jumping are very common in ETS migration patterns, and along-strike migration can happen in both directions. A prominent tremor gap is observed in midisland around 49.5°N. This gap coincides with the epicenters of the only two large earthquakes beneath Vancouver Island. ETS tremors also tend to occur in places where the local seismicity is relatively sparse. The tremor depth distribution shows a peak in the 25–35 km range where strong seismic reflectors (i.e., the E layer) are documented. Detailed waveform analysis confirms the existence of shallow tremors above the currently interpreted plate interface. Our results suggest that a significant portion of the tremor activity and perhaps associated shearing are taking place along well-developed structures such as the E layer, while fewer tremor bursts are generated elsewhere in response to the induced stress variation throughout the source volume.

Citation: Kao, H., S.-J. Shan, H. Dragert, and G. Rogers (2009), Northern Cascadia episodic tremor and slip: A decade of tremor observations from 1997 to 2007, *J. Geophys. Res.*, *114*, B00A12, doi:10.1029/2008JB006046.

1. Introduction

[2] Episodic tremor and slip (ETS) is the name given to a plate boundary phenomenon recently discovered in northern Cascadia [e.g., *Rogers and Dragert*, 2003]. It is empirically defined as "repeated, transient ground motions at a plate margin, roughly opposite to the direction of longer-term interseismic deformation, accompanied by low-frequency, emergent, semicontinuous seismic signals." Due to the nature of the three essential components of ETS events (i.e., transient ground motions, tremor-like seismic signals, and episodic occurrences), detailed ETS studies require continuous seismic and geodetic observations from a dense network over a long period of time. The first continuous GPS station in northern Cascadia was established in May 1992, and the regional seismic network completed its conversion to continuous digital recording in 1997 (Figure 1). The decade long history of continuous GPS and seismic observations provide the research community the most complete data set for detailed ETS analysis.

[3] ETS has received increasing attention from the geophysical community because it not only is an interesting natural phenomenon that may provide insights to the understanding of the mechanical behavior of earth materials as they shift from brittle (seismic) to ductile (aseismic) regimes, but also is a phenomenon that may have significant implications in the understanding of seismic hazards in subduction zones. Recent studies have shown that individual ETS episodes may have very different spatial-temporal characteristics, ranging from major events with pronounced surface displacements that migrate over hundreds of km in several weeks, to very minor ones lasting only a few hours without resolvable GPS displacements [*Kao et al.*, 2006, 2007a; *Wang et al.*, 2008]. Major ETS events in southern Vancouver Island (VI) and Washington State appear to have an average recurrence interval of 14.8 months over the last decade, but the recurrence is less regular in other part of the Cascadia [*Brudzinski and Allen*, 2007; *Dragert et al.*, 2004; *Miller et al.*, 2002; *Rogers and Dragert*, 2003]. Because the recurrence interval has a direct implication to the loading-unloading process responsible for ETS occurrences [*Dragert et al.*, 2004], it is very important to verify if the interval remains more or less a constant regardless the size and duration of each ETS episode or the interval is in fact a function of both [*Chen and Brudzinski*, 2007].

[4] It is well documented that north Cascadia ETS events migrate laterally along the strike of the subduction zone [e.g., *Kao et al.*, 2005; *Rogers and Dragert*, 2003; *Szeliga et al.*, 2008]. Based on the two major episodes in 2003 and 2004, *Kao et al.* [2006] estimate the average migrating speed to be 5–10 km/d, but acknowledge that the daily

[1]Geological Survey of Canada, Natural Resources Canada, Pacific Geoscience Centre, Sidney, British Columbia, Canada.

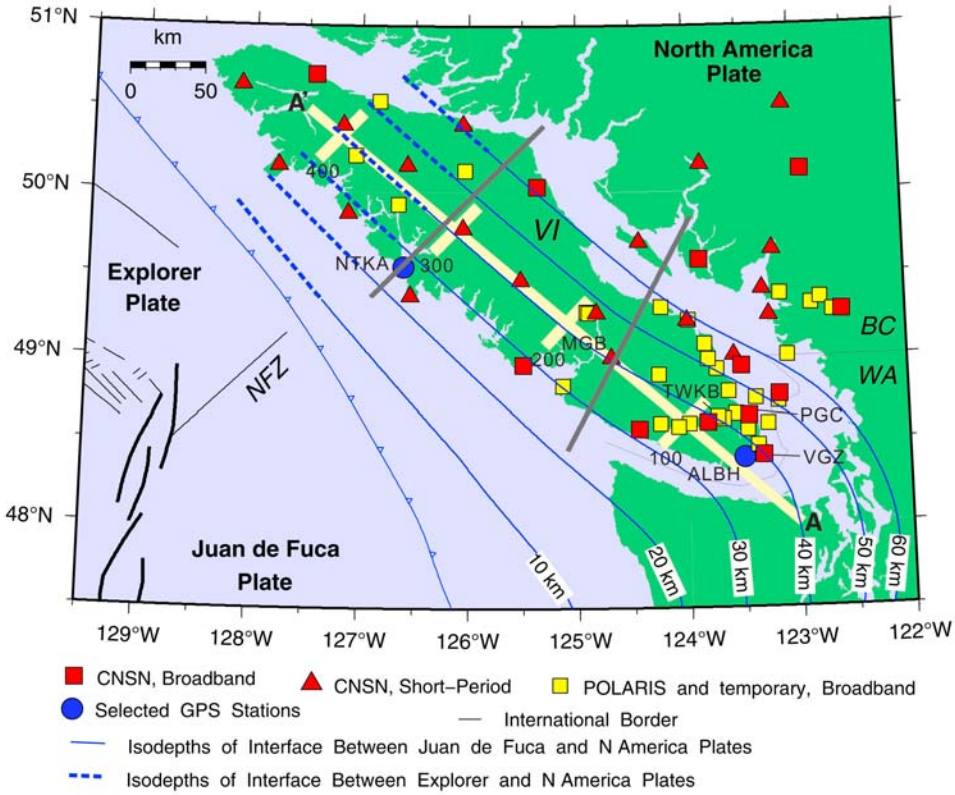

Figure 1. Map showing the general tectonic setting of the northern Cascadia region and the station distribution of regional seismic networks. Blue lines show the location of depth contours of the subducting plate interface [*McCrory et al.*, 2004]. Available seismic stations from both permanent and temporary deployments are shown as squares (broadband) and triangles (short period). Blue circles mark the two GPS stations included in this study. The Vancouver Island (VI) region is subdivided into three sections (southern, middle, and northern, as separated by the two gray lines). A–A′ marks the location of a NW–SE profile parallel to the strike of the subducted slab that is used in Figure 5 to show the along-strike distribution of tremors. The numbers (100, 200, 300, and 400) correspond to the distance (in km) from the reference point A. The Nootka Fault Zone (NFZ) is the transform boundary between the Explorer plate to the north and the Juan de Fuca plate to the south. Here BC is British Columbia, Canada and WA is Washington State, United States.

speed actually varies significantly during different stages (i.e., starting, middle, or ending) of the episodes. The migration pattern is even less regular for minor episodes, which sometimes can "jump" over a distance of 150 km or more [e.g., *Kao et al.*, 2007a]. There are many unanswered questions about the migration of ETS. For example, what physical mechanism(s) would cause ETS to migrate as opposed to occurring over a large region at the same time? What are the major factors that control the migrating speed? Do different episodes have more or less the same migration pattern if they occur in the same region? Answers to these questions require a comprehensive investigation of the spatial-temporal patterns of all available ETS events.

[5] Another fundamental issue is the exact depth of ETS fault slip. The transient surface motions, as detected by GPS measurements, can be modeled by a slow slip of several cm on the subducting plate interface between the 25 and 45 km depth contours, directly downdip from the locked zone [e.g., *Dragert et al.*, 2001; *Kao et al.*, 2006; *Wang et al.*, 2008]. Even though this model is widely accepted by the research community, the nonunique nature of the inversion of surface displacements monitored by GPS does not rule out the possibility of slip zones at different depths or shear distributed over a finite depth range [*Kao et al.*, 2006].

[6] In contrast, the depth distribution of tremor sources is a subject of controversy. Nearly all nonvolcanic tremors in the Nankai region, SW Japan, are located within a narrow zone several km above the local seismicity in the subducted crust, and are interpreted to be the result of transient shear motions on the plate interface [e.g., *Hirose and Obara*, 2005; *Ito et al.*, 2007; *Obara*, 2002; *Shelly et al.*, 2006, 2007a]. The ETS tremors in northern Cascadia and Chile are reported to occur over a wide depth range spanning from the subducted oceanic crust to the overriding continental crust [e.g., *Gallego et al.*, 2007; *Kao et al.*, 2005; *McCausland et al.*, 2005]. Whether or not the sources can occur in places other than the interface thrust zone has significant implications for the physical processes that generate ETS tremors and the associated seismic hazard [*Kao et al.*, 2006].

[7] In this study, we try to establish a comprehensive observational basis for northern Cascadia ETS tremors by analyzing continuous seismic and GPS records collected in the last decade (1997–2007). The recently developed Tremor Activity Monitoring System (TAMS) [*Kao et al.*,

2007b] and Source-Scanning Algorithm (SSA) [*Kao and Shan*, 2004] are improved and applied to the continuous seismic waveforms to delineate the spatial-temporal distribution of ETS tremors for all episodes. To facilitate a meaningful comparison of ETS tremor in different regions, we propose an "ETS scale system" to quantitatively characterize the physical dimension and duration of each episode. We also present additional evidence to address the controversial issue of tremor depths. Based on the most complete analysis of northern Cascadia ETS events so far, we propose physical models and discuss the implications of our observations.

2. Data and Analysis

[8] Continuous digital seismic waveforms from the Canadian National Seismograph Network (CNSN) constitute the principal data set used in this study. Over the past decade, many CNSN stations in the studied area were gradually upgraded from single-component, short period instruments to three-component, broadband ones. A number of new stations were installed in key locations to significantly improve the overall station coverage on VI (Figure 1).

[9] In addition to permanent CNSN stations, the semipermanent broadband stations from the BC Array of the Portable Observatories for Lithospheric Analysis and Research Investigating Seismicity (POLARIS) are included in our analysis whenever they are available (Figure 1). Beginning in early 2003, additional seismometers have been deployed at temporary sites shortly before the predicted start of a major ETS episode to increase local station coverage. In general, these temporary stations stayed in the field until at least one week after the end of that episode. No temporary data sets are available for minor episodes that occur outside the 15 month predicted time windows.

[10] There are two major components in our analysis. First, the recently developed "Tremor Activity Monitoring System" (TAMS) is applied to all waveform data to identify the approximate temporal and spatial distribution of each tremor episode [*Kao et al.*, 2007b, 2008]. Once a sufficient number of stations are classified as showing coherent tremor patterns, these waveforms are passed to the second component, which uses the Source-Scanning Algorithm [*Kao and Shan*, 2004] to determine the precise origin time and location of each tremor burst. In this section, we only briefly describe how these two methods work and what improvements we have added to enhance their performance. Readers are referred to our previous studies for the technical details of the methods [*Kao and Shan*, 2004, 2007; *Kao et al.*, 2007b, 2008].

2.1. Tremor Activity Monitoring System

[11] The original objective of TAMS is to recognize waveform patterns associated with tremor signals in a timely manner by systematically examining seismic waveforms recorded at contiguous stations. The basic design criteria of TAMS are as follows: (1) it is an automatic system that can be operated without human intervention; (2) it does not require dense station coverage for the region(s) to be monitored; (3) it is platform independent; and (4) the core algorithm must be configurable to suit a variety of regional settings (tectonic or environmental) and/or station distributions. In our case, we roughly divide the study area into three monitored regions (i.e., northern, middle, and southern VI, Figure 1).

[12] There are three major modules in TAMS: the Waveform Retrieval Module (WRM), the Waveform Analysis Module (WAM), and the Information Delivery Module (IDM). The WRM is configured to communicate with CNSN's data acquisition system to extract waveform streams from both permanent and temporary stations. Once the data retrieval process is completed, the assembled data set is passed to the WAM whose function includes a series of procedures to condition the original seismic signals, to calculate two diagnostic functions that are sensitive to the overall waveform characteristics, and to quantitatively determine the most likely waveform pattern (background noise, earthquakes/spikes, or tremor) for each hour long seismogram. The IDM handles all the postanalysis tasks such as archiving results, preparing summary reports in both text and graphic formats, and delivering them to network operators and researchers. When a high level of tremor activity is detected, an alert message is sent to a precompiled list of clients.

[13] For this study, we reconfigured the WRM to work with CNSN's waveform archive server to systematically retrieve the entire collection of digital seismograms for northern Cascadia. We also modified the algorithm used in the WAM to recognize a "coherent tremor" (CT) pattern. When a typical or possible tremor pattern (i.e., "R" or "r") is identified at a given station, instead of relying on the approximate arrival times of individual tremor bursts at nearby stations to confirm the coherency, the improved version assesses the level of similarity between this and nearby stations by calculating the corresponding cross correlation coefficients using hour long waveform envelopes decimated to a sampling interval of 10 s. The waveform pattern is reclassified from R or r to "CT" if the majority of nearby stations also have R or r patterns and waveforms recorded within a radius of 120 km are deemed highly similar (in our case, the average correlation coefficient of the decimated envelope pairs must be 0.6 or larger). An added benefit of this new approach is that the TAMS results can be used directly to select highly coherent waveform data as the input to the later tremor location process, thus increasing the resolution of our tremor solutions.

2.2. Source-Scanning Algorithm

[14] SSA was first proposed in 2004 to overcome the difficulty of locating ETS tremors without precise picking of *P* or *S* phases [*Kao and Shan*, 2004]. The basic concept is to systematically calculate the so-called "brightness" function for all possible combination of time and space in a given model space to image the likely distribution of seismic sources. The brightness of a time-location pair is defined as the average of the normalized absolute amplitudes observed at the predicted arrival times at all stations. A tremor solution is obtained if a peak is found in the brightness function, meaning that the corresponding location and time are consistent with the arrivals of large amplitudes observed by most stations.

[15] In practice, the scanning is conducted in a progressive fashion to save computational cost. The first stage

scans the entire time and space domain at 5 s and 10 km intervals, respectively. The purpose is to provide a rough but quick snapshot in pinpointing the likely time window(s) and section(s) where tremor sources exist. The next stage of scanning is initiated if the brightness value obtained in the first stage exceeds a preset threshold (in our case, 0.75). This time, the scanning is performed at 1 s and 1 km time and space intervals, respectively, but only for the time windows and volumes around the obtained solutions (±5 s; ±100 km in horizontal distance and ±40 km in depth). The solutions are subjected to the third stage of scanning at the finest resolution (0.1 s and 1 km) before final locations and origin times are determined. Notice that the progressive increase of scanning resolution is accommodated by simultaneous decrease in the scanning range (in both time and space). Thus, reprocessing waveform data with different smoothing factors for different stages is not required.

[16] Several improvements were made to the original version of SSA to enhance the robustness and resolution of our analysis. First, horizontal components are incorporated in the data processing to maximize the waveform constraints from shear wave energy. For each station equipped with three-component seismometers, we construct the waveform envelope of the maximum horizontal motion (i.e., the square root of the sum of the squares of both N and E components). This envelope is then compared to the waveform envelope of the corresponding vertical motion, and the one with a better signal-to-noise ratio is selected to be the input trace. Second, information about the absolute waveform amplitudes at different stations is used as an additional constraint in the scanning process to map the likely solutions. Here, a solution is accepted only if the station with the largest absolute amplitude happens to have the shortest epicentral distance as well (i.e., the largest amplitude is observed by the closest station). Finally, the contribution from individual stations to the calculated brightness is tracked throughout the scanning process. When the contribution from one particular station clearly dominates the calculation of the brightness function (i.e., $\geq$50%), the brightness is recalculated without the contribution from the dominating station. The purpose of this procedure is to ensure that the solutions are consistent with as many observed waveforms as possible. The solution is rejected if more than 70% of the calculated brightness comes from less than 50% of stations used in the analysis.

3. Results

[17] In this section, we present the results of both TAMS and SSA analysis for ETS events that occurred in northern Cascadia between 1997 and 2007. We begin with careful calibrations of the methods used in this study to demonstrate their applicability, robustness, and limitations. An ETS scale system is proposed to categorize individual ETS episodes based on their durations and spatial extents, followed by a comprehensive compilation of all tremor solutions. Finally, the controversial issue of tremor depths is addressed.

3.1. Calibration of Methods

[18] The accuracy and effectiveness of TAMS in detecting tremor activity have been previously demonstrated using a 3 year data set (2004–2006) [*Kao et al.*, 2007b]. The system has been carefully calibrated to be consistent with visual inspection results. In general, a region is likely to experience a major ETS episode if its daily CT ratio exceeds 20% for 3 consecutive days. Otherwise, the episode usually does not have detectable GPS signature.

[19] The performance of SSA is tested and calibrated in two ways. First, we apply SSA to the waveforms of a recorded local earthquake whose epicenter is in the general ETS tremor zone. According to CNSN earthquake catalog, the sample earthquake is located at 48.4902°N, 123.1514°W, with a depth of 26 km. Relocation of this event using a 3-D velocity model [*Ramachandran et al.*, 2005] place the source at 48.4855°N, 123.1070°W, and a depth of 24 km, which is closer to the solution reported by the Pacific Northwest Seismograph Network (PNSN) operated by the University of Washington (48.4858°N, 123.1514°W, 23 km). The corresponding SSA results are shown in Figure 2. Not only is the epicenter correctly located at the grid point closest to the 3-D solution, but also the same depth is recovered. Notice that the scanning results are completely constrained by inputted waveforms without any a priori phase picking information. In Figure 2, the portions of waveforms corresponding to solutions at different depths are shown in different colors. The time difference between arrivals from sources at different depths actually varies with epicentral distance (Figure 2). For examples, the *S* phase from a source at 14 km depth (10 km shallower than the best fitting solution) would arrive at VGZ (epicentral distance 17.3 km) ~3.8 s earlier than that from a source at 34 km (10 km deeper), but the time difference is only 0.11 s at SHB (epicentral distance 134.4 km). Therefore, a source at a shallower depth (e.g., 14 km) with a slightly delayed origin time (+1.9 s) could match the observed *S* phase at VGZ but the predicted *S* arrival is ~1.8 s late at SHB (Figure 2). Similarly, it is not possible to produce a good match for stations at all distances with a deeper and earlier source. In other words, any trade-off between the origin time and source depth can be effectively prevented if the station coverage extends over a sufficient distance range.

[20] The uncertainty of SSA solutions depends on a number of factors, such as the overall signal-to-noise ratio of the input data, the station coverage, the accuracy of the velocity model used in the travel time calculation, and the temporal and spatial intervals used in the scanning process. Generally speaking, the brightness distribution itself is a good proxy to the location uncertainty because the brightness value at each point represents how likely a source may exist, as constrained by the arrivals of large amplitudes at individual stations. *Kao and Shan* [2004] calibrated the uncertainty of a SSA solution using a synthetic data set and reported that the contour of 0.85 corresponds well to the uncertainty determined by conventional phase-picking methods. For the case shown in Figure 2, the location uncertainties in horizontal and vertical directions are ±2 and ±4 km, respectively. For tremor signals that appear to be well separated from each other, we expect the location uncertainties to be similar or slightly larger. The uncertainty would increase significantly (by a factor of 2 or more) if the tremor bursts from multiple sources are superimposed. A preliminary study applying different tremor-locating methods to the same data set suggests that SSA is particularly

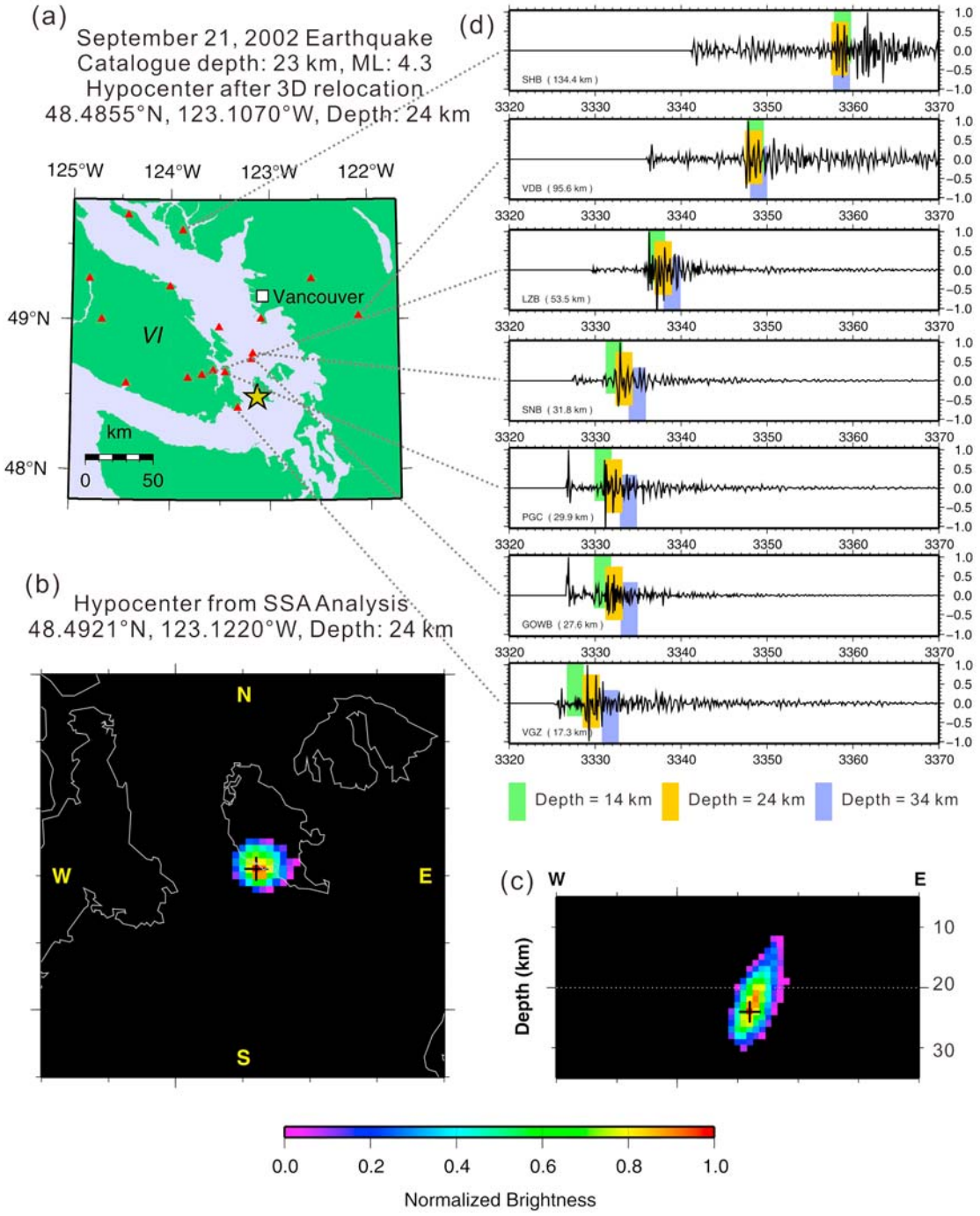

Figure 2. Calibration of the Source-Scanning Algorithm (SSA) using a local earthquake. (a) Map showing the epicenter of the event (star) and seismic stations used in the analysis (triangles). (b) SSA image of the source on a horizontal plane at the source depth. The corresponding brightness function is displayed in color. The location of maximum brightness, which is the most likely location of the source, is marked by a cross. (c) Similar to Figure 2b, but the image corresponds to an E–W vertical profile at the epicenter. Notice the consistency between the SSA and 3-D relocation results. (d) Predicted arrival times of the *S* phases at stations with different epicentral distances. Different colors correspond to solutions at different depths. It is clear that a solution at 24 km fits the waveform data best. Because the time difference between arrivals from sources at different depths actually varies with epicentral distance, the trade-off between origin time and source depth is effectively eliminated.

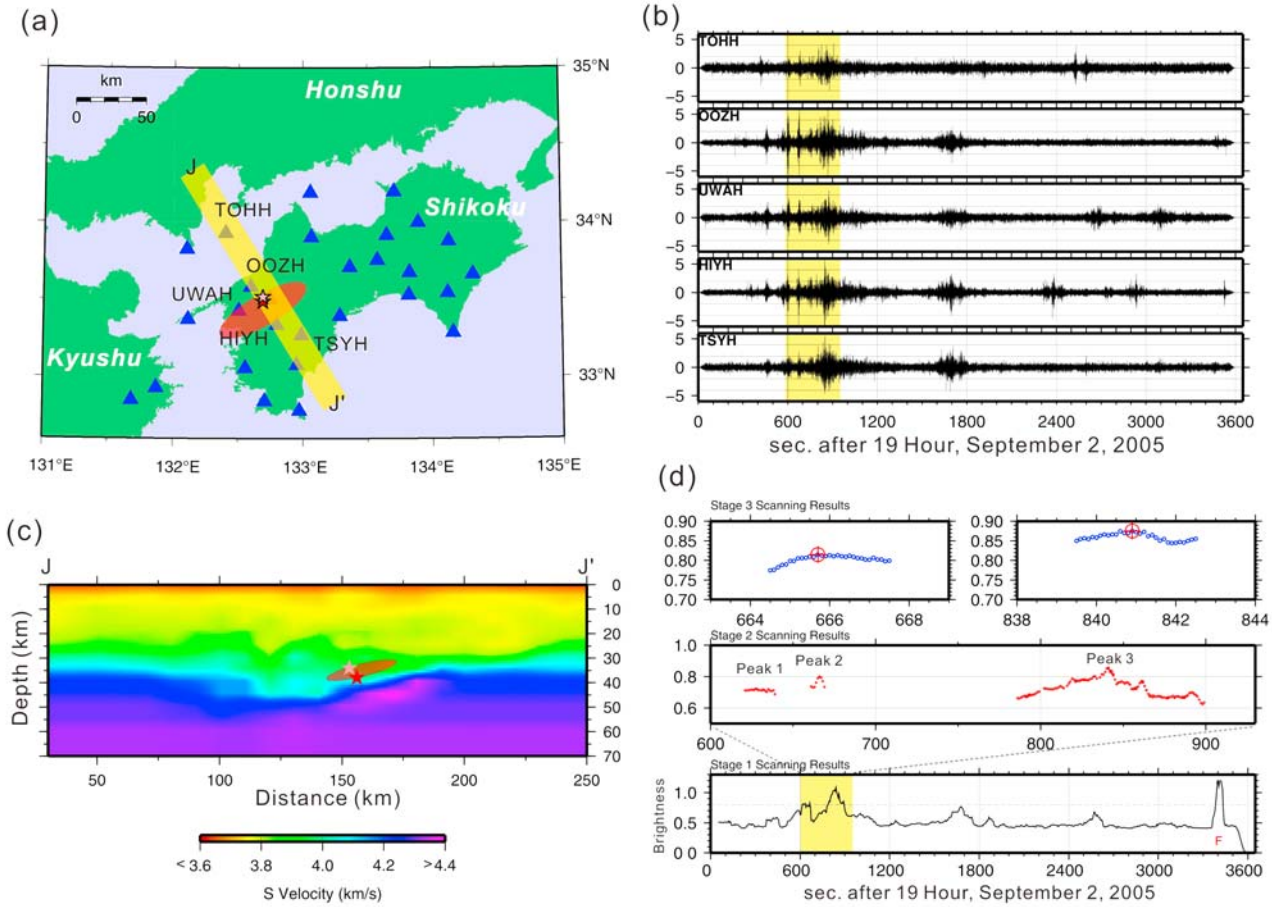

Figure 3. Calibration of the SSA using a 0.5 hour tremor data set from SW Japan. (a) Map showing the locations of seismic stations used in the analysis (triangles), epicenters of the two tremor solutions (red and pink stars), the general epicentral area of tremors (orange oval) reported by *Shelly et al.* [2006], and the location of cross section (J–J′, yellow area). (b) Representative examples of normalized waveforms. Segments corresponding to the two tremor solutions are highlighted. (c) NW–SE cross section showing the two tremor solutions (stars), the shear wave velocity structure (color scale), and the general area of tremors (orange oval) reported by *Shelly et al.* [2006]. Notice that both tremor solutions are consistent with the location of previously determined tremor cluster. (d) Results of the three-stage scanning using SSA. The entire waveform traces are scanned in stage 1 (at the spatial interval of 10 km and a time step of 5 s). An "F" is marked beneath a solution if its brightness calculation is dominated by a small number of stations. Solutions with brightness >0.8 are selected to enter the next stages of scanning with increasing time and space resolution. The final solutions are marked by the target symbols.

effective in delineating tremor clusters whose source locations are not stationary [*Hirose et al.*, 2006]. A joint study that systematically addresses the strength, weakness, and associated uncertainty of each method is currently underway (K. Creager, personal communication, 2009).

[21] Second, we apply SSA to tremor data whose solutions have been determined by other studies with independent methods. Here, nonvolcanic tremors in SW Japan are chosen because of the following four reasons: (1) the seismic station density in SW Japan is among the highest in the world; (2) high-quality waveform data are efficiently maintained and distributed by the National Research Institute for Earth Science and Disaster Prevention (NEID) of Japan [*Obara et al.*, 2005]; (3) the tectonic setting and high-resolution 3-D velocity structures of SW Japan are well known and available; and most importantly; and (4) the nonvolcanic tremors in SW Japan have been extensively studied with precisely determined locations and depths. We process a small subset of the waveforms analyzed in two previous studies [*Shelly et al.*, 2006, 2007a] and adopt the identical 3-D velocity model. The same SSA scanning procedures as outlined above are applied without any alteration.

[22] Figure 3 shows the SSA results for the tremor samples in SW Japan. To fully demonstrate the SSA's remarkable ability of noise tolerance, three-component, hour long waveforms from the entire data set (27 local broadband seismic stations in total) are included in the analysis without any quality prescreening, although in principle, waveforms with low signal-to-noise (S/N) ratios should be removed to increase SSA's resolution [*Kao and Shan*, 2004].

[23] Two tremor solutions were obtained after all 3 stages of SSA scanning. The brightness function of the first stage

Table 1. A Proposed Scale System for Episodic Tremor and Slip

Class	Corresponding Physical Meaning
Index for Spatial Size	
A	Lateral dimension ≥300 km
B	Lateral dimension between 150 and 300 km
C	Lateral dimension between 50 and 150 km
D	Lateral dimension <50 km
Index for Total Duration	
4	Episode lasting longer than 3 weeks
3	Episode lasting between 2 and 3 weeks
2	Episode lasting between 1 and 2 weeks
1	Episode lasting between 3 days and 1 week
0	Episode lasting less than 3 days
Index for Migration Pattern	
N	Northward
S	Southward
B	Bilateral
H	Halting
J	Jumping

shows 4 segments (at ∼630 s, ∼660 s, ∼840 s, and ∼3400 s) with values exceeding 0.75. The last segment does not enter the next stage of scanning because the calculated brightness is dominated by a small number of stations (as marked by an "F" beneath the brightness function, Figure 3d). Scanning for the first and second segments is combined in the third stage because their time difference is less than 1 min. Both final solutions locate in the tremor cluster identified by *Shelly et al.* [2006] and interpreted by them to represent the interface thrust zone (Figure 3).

3.2. An ETS Scale System

[24] Previous studies of northern Cascadia ETS events have clearly pointed out the variability in time duration and spatial distribution of individual episodes [e.g., *Brudzinski and Allen*, 2007; *Kao et al.*, 2006, 2007a; *Szeliga et al.*, 2008]. The variability can be even more significant if episodes from other parts of the Cascadia margin (or other subduction zones) are involved. Before we proceed to presenting the detailed spatial and temporal characteristics of individual ETS events in the last decade, a simple scale system is proposed to establish a more quantitative way of characterizing the size of an ETS event.

[25] Our proposed ETS scale system is summarized in Table 1. For each episode, one alphabetic letter and one digit are used to represent its approximate spatial dimension and time duration, respectively. The starting date of each episode is defined as the first day when the CT ratio of one or more sections (i.e., southern, middle, or northern VI) exceeds 20%. An episode is considered "finished" if the daily CT ratios of the next 15 days all fall below 20%. The daily geographic centers of tremor clusters are used to depict the migration characteristics of each episode, and the distance between the northernmost and southernmost daily centers is used to define the spatial dimension of an episode. Such derived temporal and spatial dimensions are deemed representative of the bulk characteristics of an episode with minimum effects from a few outliers.

[26] From a practical/empirical point of view, the ETS scale categorizes individual events into four classes (A, B, C, and D). An episode is categorized as A class if the corresponding lateral dimension (i.e., the length projected onto the strike of the margin) is ≥300 km. Similarly, a B class episode would have a lateral dimension between 150 and 300 km. Episodes with lateral dimension between 50 and 150 km are considered C class, while the last class (D) is referred to episodes with lateral dimension <50 km.

[27] An implicit assumption in measuring the lateral dimension of an episode is that it is more or less spatially continuous. However, as documented by *Kao et al.* [2007a], the observed tremor activity may jump over some distance to a neighboring section. Also, as we shall illustrate in more detail later, it appears to have a gap in the tremor distribution beneath mid-Vancouver Island. Consequently, when two tremor clusters occur successively in time (or even simultaneously) but separated in space, it may become ambiguous to group them into the same episode or treat them as two independent (smaller) ones. Since we roughly divide our study area into three sections of about the same dimension (∼150 km each), we set the threshold of "jumping distance" to be one half of the section length (i.e., 75 km). In other words, two independent episodes are recognized if the spatial gap in between is ≥75 km.

[28] We use the number of weeks to characterize the time duration of an ETS episode. For examples, 0 is assigned if an episode lasts less than 3 days. Similarly, 1, 2, or 3 are given to episodes with total durations up to 1, 2, or 3 weeks, respectively. We use the number "4" for events longer than 3 weeks. Because northern Cascadia ETS events rarely persists much longer than 4 weeks, adding more classes for this region are unnecessary and less practical.

[29] Our proposed ETS scale system is designed to give a quick, first-order description of the physical size of an ETS event. It can be supplemented by adding more indices to characterize other features of interest. One example is to use another letter to denote the observed migration pattern (from south to north, from north to south, bilateral, halting, or jumping). The equivalent moment magnitudes can also be considered although current estimates are based on lateral dimensions of the observed ETS events.

3.3. ETS Recurrence

[30] The 10 year TAMS results are summarized in Figure 4. In Table 2, we list the basic parameters for all ETS episodes with C class or above. The spatial and temporal distribution of all tremor solutions, with respect to the strike of the margin, is shown in Figure 5 together with continuous GPS observations at two stations in northern and southern VI. Different classes are marked by different colors and symbol sizes.

Figure 4. Daily summaries of the Tremor Activity Monitoring System (TAMS) for the past decade (1997–2007). The Vancouver Island region is roughly divided into the following three sections: northern, middle, and southern (boundaries marked in Figure 1). (top) The daily percentage of hours showing coherent tremor (CT) pattern for each section is marked by a thick red line and the number of seismic stations available for automatic classification is shown by a blue line. (bottom) Regular recurrence of major episodic tremor and slip (ETS) events is best displayed after applying a low-pass (20 days) filter.

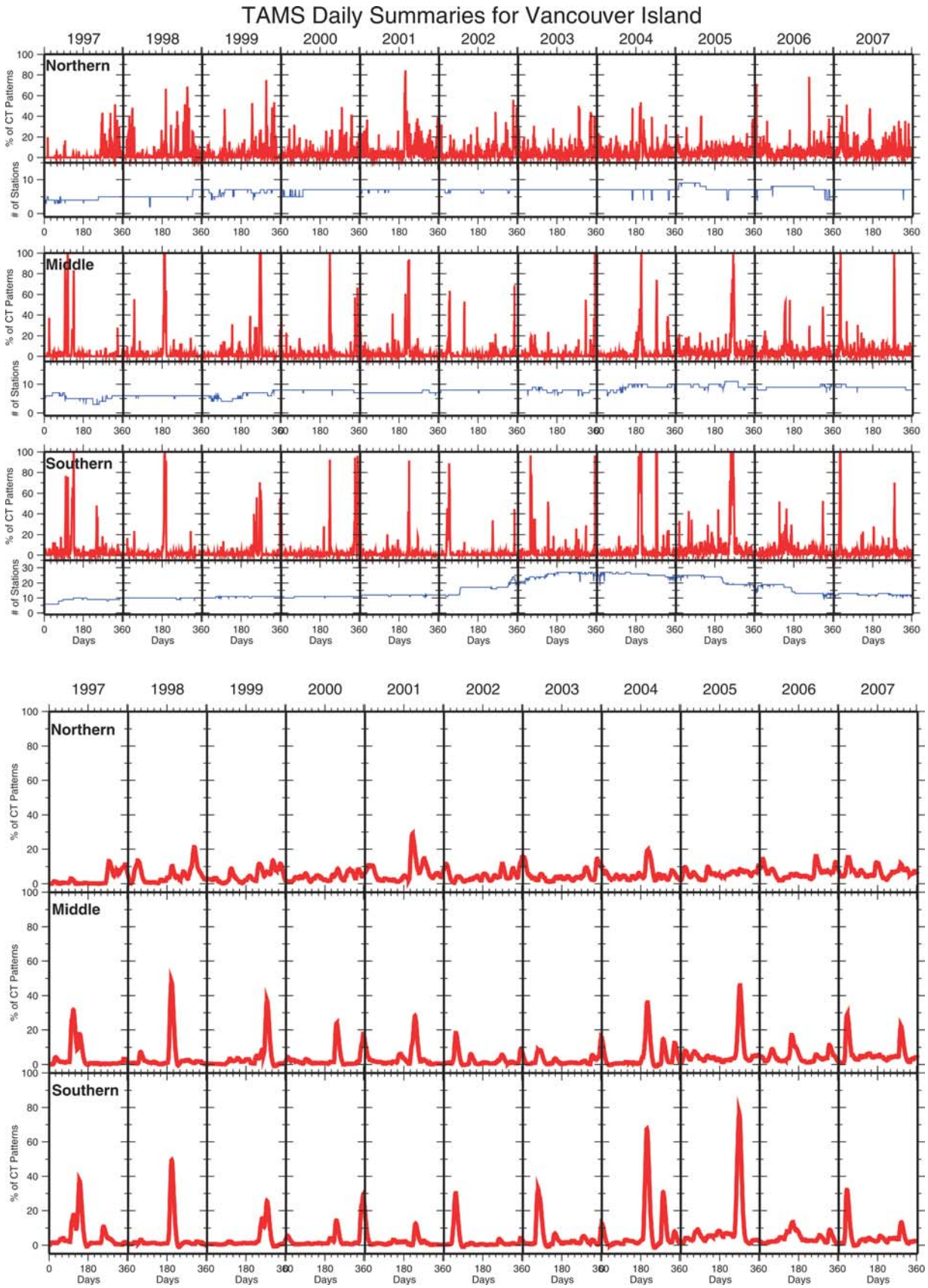
TAMS Daily Summaries for Vancouver Island
1997
1998
1999
2000
2001
2002
2003
2004
2005
2006
2007
Northern
Middle
Southern
% of CT Patterns
# of Stations
Days

Figure 4

Table 2. Summary of North Cascadia Episodic Tremor and Slip Events[a]

Starting Date	Total Duration (days)	Region[b]	Class[c]	Migration Pattern[c]	Moment Magnitude[d]
		A Class Episodes			
6 Apr 1997	42	S/M/N	A4	B, H, J	–
9 Aug 1999	55	S/M/N	A4	B, H, J	6.7
23 Jul 2001	25	M/N	A4	S, H	–
28 Nov 2003	29	M/N	A4	H, J	–
1 Jul 2004	42	S/M/N	A4	N, H, J	–
5 Sep 2005	23	S/M	A4	N, H	6.7
		B Class Episodes			
4 Jul 1998	15	S/M	B3	S	6.8
15 Jul 2000	36	M	B4	N, H	–
3 Dec 2000	32	S	B4	N, H	6.7
4 Feb 2002	19	S	B3	N, H	6.6
26 Feb 2003	22	S	B4	N, H	–
15 May 2006	36	M	B4	N, J	–
24 Jan 2007	37	S/N	B4	H, J	6.8
4 Oct 2007	7	M/N	B1	S, H, J	–
		C Class Episodes			
19 Feb 1998	3	M	C1	H	–
5 Sep 2002	14	S/N	C2	J, H	–
8 Dec 2002	19	M/N	C3	J, H	–
9 Nov 2003	2	M	C0	S	–
30 Sep 2004	6	S	C1	H	–
20 Nov 2004	8	M	C2	H	–
7 Sep 2006	4	N	C1	H	–
9 Nov 2006	4	M	C1	N	6.2
14 Jun 2007	4	N	C1	H	–

[a]All episodes must be C class or higher.
[b]Here S, M, and N, are the southern, middle, and northern sections of Vancouver Island, respectively. Multiple regions are listed if an episode migrates over 50% of neighboring sections.
[c]Indices are defined in Table 1.
[d]Values reported in the literature [*Dragert et al.*, 2001, 2004; *Wang et al.*, 2008] and by K. Wang (manuscript in preparation, 2009).

[31] The most striking feature is the correlation between GPS and seismic signatures of major ETS episodes beneath southern VI (Figure 5), as first pointed out by *Rogers and Dragert* [2003]. For most minor episodes, however, the GPS signature is not as obvious as the corresponding tremor activity. It is unclear whether the lack of one-to-one correspondence is a result of detection threshold of the GPS network or the absence of slip at depth. For the middle and northern sections of VI, the coverage of continuous GPS monitoring becomes too sparse to consistently delineate a good correlation with respect to seismic observations (Figure 5). Densification of the GPS network in the north is obviously needed.

[32] The recurrence of major ETS episodes beneath the southern section of VI is remarkable. Out of the 14 class A or class B episodes included in our analysis, 9 of them involve at least half of the southern section of VI. The recurrence interval is estimated to be 447 ± 43 days based on parameters listed in Table 2, which is identical to the interval based on GPS data from 1994 to 2004 at ALBH (Figures 1 and 5) [*Dragert et al.*, 2004]. For the middle and northern sections of VI, the regularity of recurrence is less obvious.

[33] By constraining an ETS event to the interpreted plate interface [*McCrory et al.*, 2004], the size and spatiotemporal distribution of the slip can be inverted from GPS measurements [e.g., *Dragert et al.*, 2001, 2004]. Unfortunately, the inversion is only possible for events in the southern section of VI where GPS station coverage is adequate. In Table 2, we list the equivalent moment magnitudes of ETS events available in the literature [*Dragert et al.*, 2001, 2004; *Wang et al.*, 2008] and from K. Wang (manuscript in preparation, 2009). The limited number of samples prevents us from delineating a quantitative relationship between the class of an ETS episode and its equivalent moment magnitude. Nevertheless, it is inferred that the M_w of an A or B class episode (6.7 ± 0.1) exceeds that of a C class episode by about 0.5 or more.

[34] As pointed out by previous studies, a significant portion of tremor activity occurred outside of the regular 15 month time windows of recurrence [*Kao et al.*, 2006; *Rogers and Dragert*, 2003]. Our analysis estimates that about 50% and 30% of all tremor activities are observed during A and B class episodes, respectively. The remaining 20% are associated with minor episodes that often last from only a few hours to several days. From a statistical point of view, regular recurrence of minor episodes cannot be established with confidence.

3.4. Along-Strike Migration

[35] The speed of ETS migrating along the strike of the Cascadia margin has been estimated to vary from 5 to 15 km/d [e.g., *Dragert et al.*, 2004; *Kao et al.*, 2006]. A more recent study points out that, in addition to steady migration, the tremor activity can exhibit halting behavior (i.e., staying in a particular place for a certain period of time, often several days with a diminished level of activity) and/or jumping (i.e., the tremor cluster reappears in a different place, sometimes as far as 150 km away, without any events in between) [*Kao et al.*, 2007a]. This compilation of a decade of ETS data allows us to examine aspects of the migration in greater detail.

[36] Figure 6 shows the along-strike movement of tremor activity for all six A class episodes listed in Table 2. Only

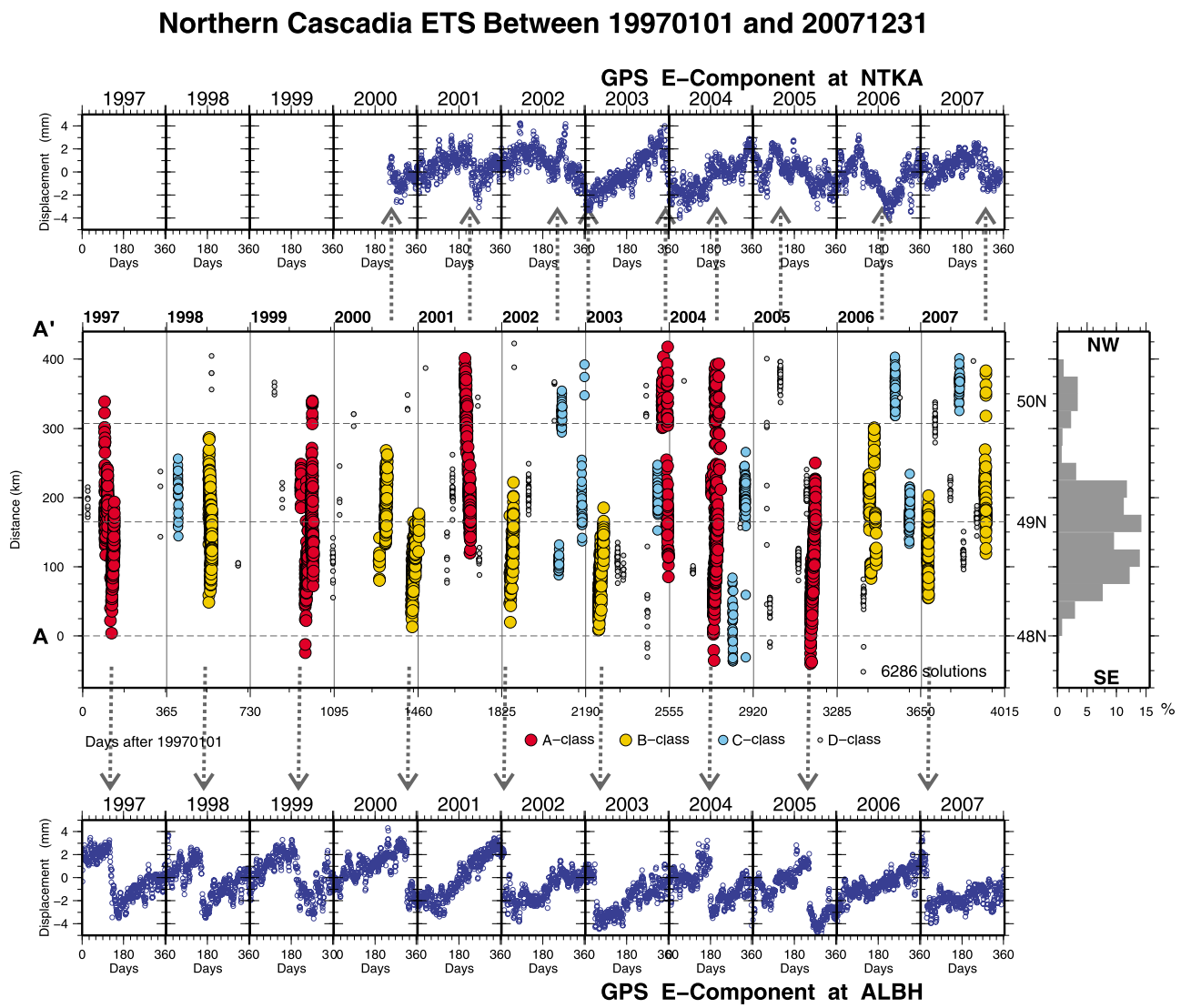

Figure 5. Spatial-temporal distribution of ETS events observed in northern Cascadia between 1997 and 2007. Each tremor solution is projected onto a NW–SE profile roughly parallel to the strike of the subducted slab (profile A–A′ in Figure 1). Episodes in different classes (as defined by Table 1 and listed in Table 2) are shown in different colors and symbol sizes. Daily GPS measurements (E component after removing long-term trend) at stations ALBH and NTKA (locations marked in Figure 1) are marked by small blue circles, showing good correlation between slip and tremor signals (as indicated by dashed gray arrows).

when tremor activity is tracked continuously without jumps or large time gaps do we consider the migration velocity to be physically meaningful. The September 2005 episode is a well-resolved example of ETS migration from southeast to northwest (Figure 6a). The initial migration speed is slow (∼5.5 km/d) with a brief halting phase. After about 2 weeks, the tremor cluster started moving at a much faster speed of ∼12 km/d. The average migration speed for the entire episode is 8.3 km/d, but the observed change in speed is statistically significant and is in need of a physical explanation.

[37] The July–August 2004 episode also has a pattern of steady northwestward migration (Figure 6b) with an average migration speed of 9.4 km/d. However, it appears that

Figure 6. Along-strike migration patterns for six A class ETS episodes in northern Cascadia. (a) September 2005 episode, (b) July–August 2004 episode, (c) July–August 2001 episode, (d) April–May 1997 episode, (e) August–October 1999 episode, and (f) November–December 2003 episode. Each tremor solution is marked by a small circle in different colors depending on its depth. The overall along-strike distribution (i.e., projecting on to profile A–A′ in Figure 1) is shown to the right of each episode. Solid blue arrows mark the time periods in steady migration (average migration speed is given). Some tremors were apparently triggered by an $M_w \sim 6.4$ earthquake offshore west of the northern VI (star) during the 2004 ETS episode.

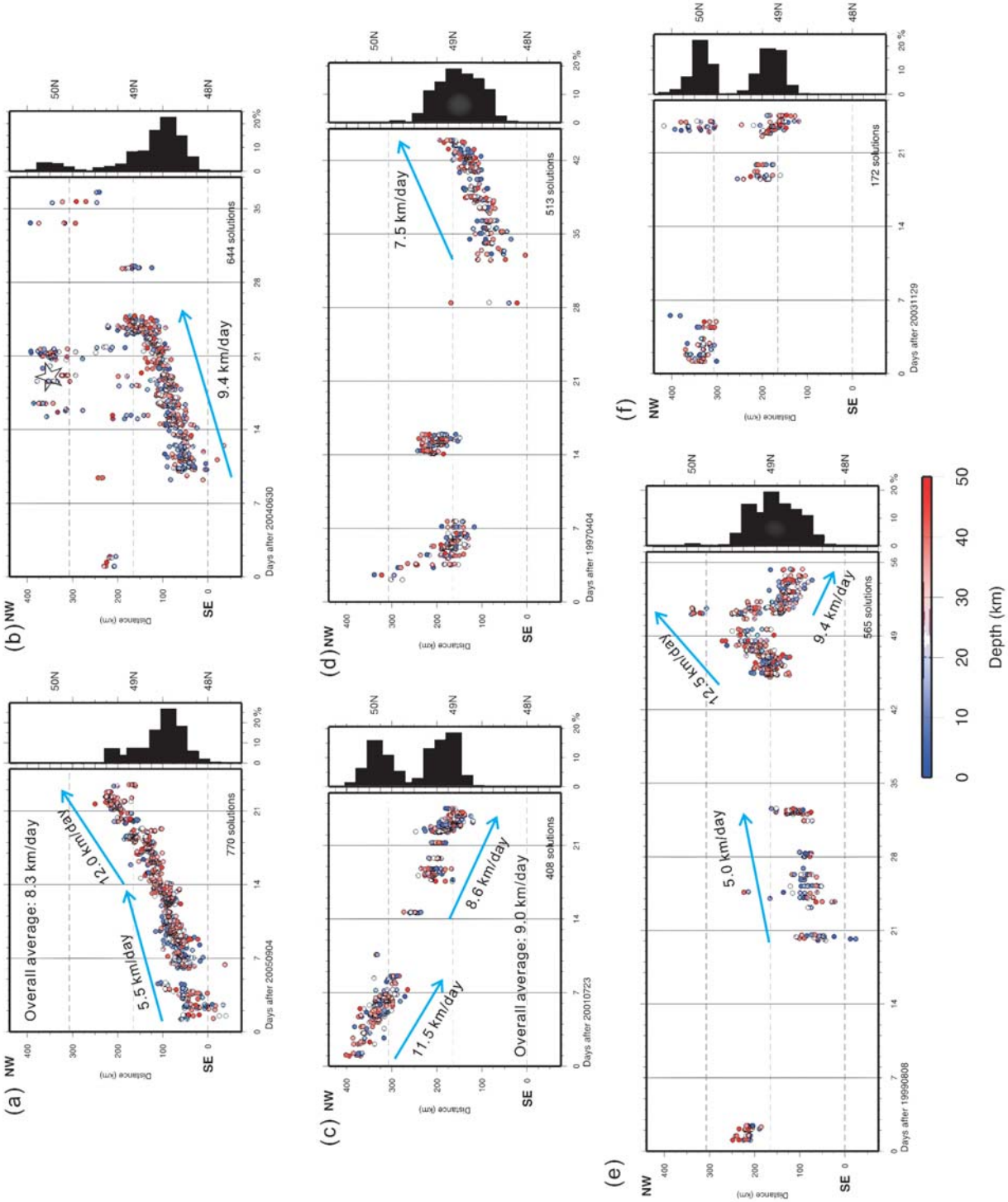
(a)
Overall average: 8.3 km/day
12.0 km/day
5.5 km/day
770 solutions
Days after 20050904
(b)
9.4 km/day
644 solutions
Days after 20040630
(c)
Overall average: 9.0 km/day
11.5 km/day
8.6 km/day
408 solutions
Days after 20010723
(d)
7.5 km/day
513 solutions
Days after 19970404
(e)
12.5 km/day
5.0 km/day
9.4 km/day
565 solutions
Days after 19990808
(f)
172 solutions
Days after 20031129
NW
SE
Distance (km)
50N
49N
48N
Depth (km)
0
10
20
30
40
50

Figure 6

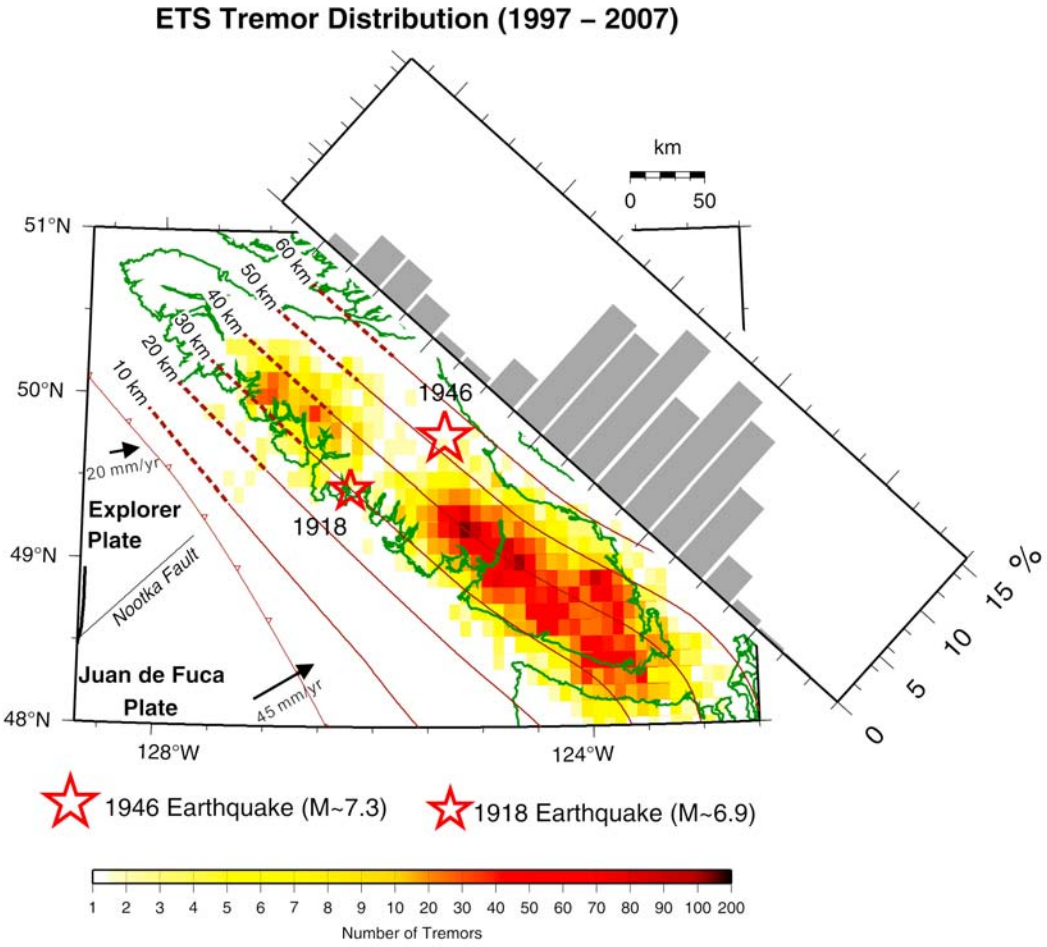

Figure 7. Map view of the occurrence density of ETS tremors in northern Cascadia between 1997 and 2007. A prominent gap is observed in the source area of the two largest crustal earthquakes in the past 150 years (stars). The overall tremor occurrence density in the southern and middle sections of Vancouver Island is about 5 times higher than that in the north, as indicated by the overall along-strike distribution of all tremor solutions.

the occurrence of an $M_w \sim 6.4$ earthquake offshore west of the northern VI on July 19, 2004, may have spurred some tremor activity well away from the main migration path. This episode therefore also provides a good example of simultaneous tremor activity in separated regions.

[38] The July–August 2001 episode is of particular interest since it shows a rare pattern of southeastward migration (Figure 6c). Starting near the northern edge of the subducted slab (Figure 1), this episode moved at a speed of 11.5 km/d toward the middle section of the island. This initial tremor activity is followed by a 7 day gap before the episode regained strength beneath mid-VI and continued its southeast migration. It is interesting to note that the overall migration speed of this episode is also 9 km/d, suggesting that the speed is not affected by the sense of direction of the along-strike migration.

[39] The remaining three A class episodes (April–May 1997, August–October 1999, and November–December 2003), although containing some continuous tremor segments, are characterized by bursts of tremor in different locations. Whether these bursts are random or linked by stress propagation cannot be resolved at this stage. The contained continuous segments for these episodes also exhibited migration speeds in the range of 5.0 to 12.5 km/d allowing us to conclude that this range may be characteristic for the tectonic environment of the northern Cascadia margin.

3.5. Epicentral and Depth Distributions

[40] A tremor density map showing the number of tremor solutions per unit area of 0.1° by 0.1° is shown in Figure 7. We also project all solutions onto a NW–SE profile passing through the axis of VI to show the along-strike variation of tremor occurrences. Eight vertical profiles sampling the entire VI from south to north are constructed to show the depth distribution of tremor occurrences and its relationship with respect to local seismicity (Figure 8).

[41] The tremor distribution extends to the northernmost edge of the Cascadia subduction system. We observe no tremors farther north where the subducted slab is absent [*Cassidy et al.*, 1998], confirming the conclusion of an earlier study based on a much smaller data set [*Kao et al.*, 2007a]. Such a correlation suggests that Cascadia ETS is closely related to subduction processes. The appearance of

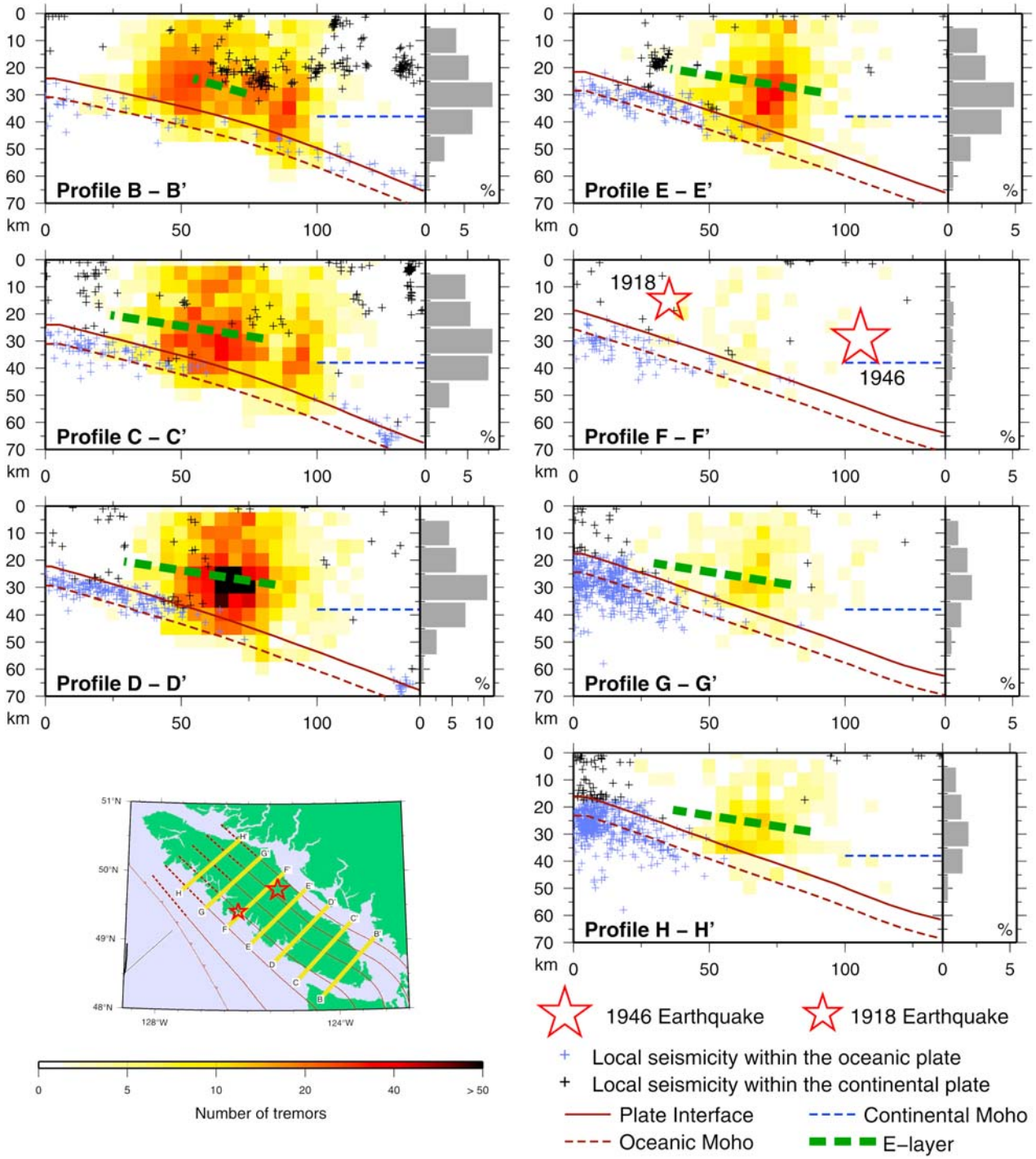

Figure 8. Occurrence density of ETS tremors and local seismicity along various cross sections of Vancouver Island. Tremor solutions and earthquake hypocenters within 15 km from the location of each profile (as marked on the map in the lower left corner) are used to avoid any distortion from projecting over a large distance. For each profile, the overall depth distribution is plotted to the right as a percentage. Peak tremor occurrence generally lies in the 25–35 km depth range (~10 km above the plate interface interpreted by *McCrory et al.* [2004]) where strong seismic reflectors (i.e., the E layer (green dashed lines)) are observed. Approximate thickness of the continental crust is adopted from *Mooney et al.* [1998].

fewer tremors to the south of the United States–Canada border, however, is an artifact due to the station distribution of CNSN (Figures 1 and 7). In fact, many major ETS episodes originate in Washington State and migrate northward across the border [e.g., *Brudzinski and Allen*, 2007; *Kao et al.*, 2006; *McCausland et al.*, 2005; *Melbourne et al.*, 2005; *Schwartz and Rokosky*, 2007].

Table 3. Average Nearness Between Different Types of Seismic Events in Northern Cascadia

Types	Profile (km)							
	A–A′	B–B′	C–C′	D–D′	E–E′	F–F′	G–G′	H–H′
Tremor–Tremor	1.2	0.7	0.8	0.7	1.0	2.8	1.8	1.6
Tremor–Crustal Earthquake	6.6	9.9	9.0	11.7	17.5	12.6	17.1	20.1
Tremor–Intraslab Earthquake	13.8	14.4	16.9	16.4	17.4	18.0	16.5	22.4
Crustal Earthquake–Crustal Earthquake	0.9	1.3	1.7	4.4	1.4	6.6	3.9	2.2
Intraslab Earthquake–Intraslab Earthquake	2.1	2.9	1.8	1.0	1.2	1.6	0.9	0.8

[42] Our results indicate that the level of tremor activity is definitely uneven beneath VI. Patches with the highest tremor occurrence are found beneath the middle and southern sections of VI, while the peak occurrence density decreases by a factor of 5 in the north. The along-strike profile shows a prominent tremor gap at the boundary between the middle and northern sections of VI (~49.5°N, Figure 7). To the south of this gap, the surface projection of ETS tremors closely follows the geometry of the subducted Juan de Fuca plate (JDF), and is bounded approximately by the 30 and 50 km contours of the interpreted plate interface. The distribution shifts seaward to the north of the gap where the younger Explorer plate (EP) is subducting beneath the North America plate at a slower rate [*Braunmiller and Nábelek*, 2002] (Figure 7). It is important to note that the approximate location of the gap does not coincide with the landward extension of the present JDF–EP plate boundary (Nootka fault, Figure 7), but is ~50 km to the south.

[43] Perhaps the most intriguing feature of the observed tremor gap is that it coincides remarkably well with the epicenters of the only two large earthquakes beneath VI (the 1918 *Ms* ~ 6.9 and 1946 *Ms* ~ 7.3 earthquakes, Figure 7) since European settlement was established more than 150 years ago. In spite of the sparseness of seismic data and felt reports, the source characteristics of these two events were reasonably constrained from a combined data set of historical seismograms, seismograph station reports of first arrivals, local intensity distributions, and reports of water disturbances [*Cassidy et al.*, 1988; *Hasegawa and Rogers*, 1978; *Rogers and Hasegawa*, 1978; *Rogers*, 1983]. All available data suggest that both events are shallow (~15 km for the 1918 event and ~30 km for the 1946 event) with strike-slip focal mechanisms [e.g., *Cassidy et al.*, 1988; *Rogers and Hasegawa*, 1978]. We estimate the lateral dimension of the tremor gap to be 20–30 km, which is on the same order as the source size of these two large events.

[44] The spatial correlation between the tremor gap and large crustal earthquakes is also evident on the vertical profile F–F′ shown in Figure 8. In fact, there is an overall trend that tremors tend to occur in places where the local seismicity within the overriding crust is relatively sparse (Figure 8). Such a trend is best characterized by comparing the "tremor–earthquake" nearness (defined as the minimum distance from a tremor source to nearby earthquakes), the "tremor–tremor" nearness (the minimum distance from a tremor source to nearby tremors), and the "earthquake–earthquake" nearness (the minimum distance from an earthquake to nearby earthquakes) [*Kao et al.*, 2005]. To make our assessment more specific, the local seismicity is further grouped into two categories, crustal and intraslab, depending on their positions relative to the inferred plate interface (Figure 8 and Table 3).

[45] For profiles south of the tremor gap (B–B′, C–C′, D–D′, E–E′), the average tremor–tremor nearness is 1 km or less, whereas the average earthquake–earthquake nearness (either crustal–crustal or intraslab–intraslab) ranges from 1 to 4.4 km. In contrast, the average tremor–earthquake nearness is much larger, ranging from 9 km along the profile C–C′ to 17.5 km along the profile E–E′. Quantitatively, these nearness values imply that tremors tend to occur in tight clusters, and so do local seismicity. But for any given tremor location, the distance to a nearby earthquake hypocenter is on average 10 times greater than the distance to a neighboring tremor. Similar patterns are observed for northern profiles (F–F′, G–G′, and H–H′) with slightly larger tremor–tremor nearness values (due to fewer tremors, Table 3 and Figure 8). In other words, the mutually exclusive relationship between the spatial distributions of tremors and local seismicity appear to be persistent throughout VI.

[46] As far as the depth distribution of ETS tremors is concerned, no significant difference on both sides of the gap can be discerned. The peak tremor occurrence is observed at the depth of 25–35 km for all profiles with the number of tremors decreasing both upward and downward (Figure 8). An important aspect of the tremor depth distribution is its spatial correlation with the strong seismic reflectors that are identified from regional seismic reflection profiles [*Clowes et al.*, 1987; *Hyndman*, 1988; *Spence et al.*, 1985]. These reflectors, often referred to as the E layer, also correspond to low shear wave velocity [*Cassidy and Ellis*, 1993] and relatively high electric conductivity [*Hyndman*, 1988]. The E layer has been interpreted as an extensive shearing deformation zone that traps a significant amount of fluids released from dehydration reactions of subducted materials below the plate interface [e.g., *Hyndman*, 1988; *Nedimovic et al.*, 2003; *Peacock*, 1990], as an underplated sliver [*Clowes et al.*, 1987], or as the subducted oceanic crust itself [*Nicholson et al.*, 2005]. Our results show that the depth of peak tremor occurrence coincides with the inferred locations of the E layer beneath both north and south VI (Figure 8). Furthermore, the majority of tremors and the E layer are located in the same distance range from the trench axis. For the two profiles in southern VI (profiles B–B′ and C–C′), a second patch of high tremor occurrence is observed farther downdip near the tip of the mantle wedge (Figure 8).

4. Implications and Discussion

4.1. Anticorrelation Between Tremors and Local Seismicity

[47] The physical causes for the observed depth distribution of Cascadia ETS tremor activity and its apparent anticorrelation with local seismicity are not yet understood.

One qualitative explanation may be that the mechanical/rheological conditions that facilitate the occurrence of ETS tremors may discourage the occurrence of ordinary earthquakes, and vice versa. Under such a scenario, both ETS tremors and ordinary earthquakes are manifestations of a stress releasing process in the crust. In places where fluids are abundant, the combined effects of a high pore pressure (thus low effective rock strength) and finite fluid inclusions (thus limited rupture length) would favor the occurrence of tremors as soon as the stress regime is above the critical state. The consequence of such quasicontinual release of the accumulated stress through tremors is therefore responsible for the lack of ordinary earthquakes. A corollary of this would be the existence of anomalous crustal stress gradients at the boundaries of the tremor regions which may be resolvable through shear wave splitting studies.

4.2. Significance of the Tremor Gap

[48] The above logic can be used to explain the coincidence of the tremor gap and the two largest earthquakes beneath mid VI (Figures 7 and 8). From the aspect of accumulation/releasing of crustal stress, there are at least two ways to explain the observed pattern. The first one is that the lack of tremors is equivalent to the lack of mechanisms to release accumulated stress. Therefore, the tremor gap is a marker for an area that is marching toward the next large earthquake. The second scenario is that the occurrence of two large earthquakes in the relatively recent past could have significantly reduced crustal stress and/or fluid pore pressure, thereby inhibiting tremor activity in this region for some period of time. The implication of such an alternative, however, is that instead of using the tremor gap as a marker for large earthquakes, it points to a region of temporarily reduced seismic hazard. Exactly how long the tremor gap would need to regain its strength depends on the accumulation rate of tectonic stress in the source region.

[49] With the present knowledge, whether or not the observed tremor gap is a time-variant phenomenon cannot be determined. According to a recent analysis of GPS and geological data for northern Cascadia, the recurrence intervals of forearc crustal earthquakes with $Mw > 6$ and $Mw > 7$ are 45 and 400 years, respectively [*Hyndman et al.*, 2003]. Detailed reexamination of marine sediment records over the past 4000 years also confirms the average recurrence interval of large earthquakes beneath southern VI to be ~400 years [*Blais-Stevens et al.*, 2009]. If the level of tremor activity is indeed linked to the recurrence cycle of large crustal earthquakes, then a tremor gap beneath southern VI is expected in the future as the next large event gradually approaches. On the other hand, if the tremor gap is related to rheological/mechanical conditions unique to the local tectonic/geological setting in mid-VI, then large crustal earthquakes may still occur in southern VI without the development of a tremor gap. The limited history of seismic and tremor observations in this region prevents us from distinguishing the two possibilities at this time.

[50] The available data sets for both 1918 $Ms \sim 6.9$ and 1946 $Ms \sim 7.3$ earthquakes might have prevented a detailed investigation of their rupture history, but their basic source parameters (i.e., origin time, epicenter, depth, and magnitude) were reasonably constrained [*Cassidy et al.*, 1988; *Hasegawa and Rogers*, 1978; *Rogers and Hasegawa*, 1978; *Rogers*, 1983]. Taking the 1918 event for example, the epicenter and origin time were estimated from 49 first arrival times with an uncertainty of 30 km [*Cassidy et al.*, 1988]. Its depth was determined to be shallow (best fit at 15 km with bounds of 5 and 20 km) based on forward modeling of surface wave radiation patterns and the abundance of aftershocks [*Cassidy et al.*, 1988; *Page*, 1968]. The 1946 event was located deeper (30 ± 10 km) in the lower crust of the overriding North America plate [*Hasegawa and Rogers*, 1978; *Rogers and Hasegawa*, 1978; *Rogers*, 1983]. Such an inference is consistent with the observation of very few aftershocks [*Hodgson*, 1946] and modeling results of near-field ground deformation [*Rogers and Hasegawa*, 1978]. It is interesting to point out that even though tremor occurrence in the gap zone is rare (<1%), the anticorrelation between tremors and local seismicity remains unaltered (profile F–F′, Figures 7 and 8 and Table 3).

[51] Both northern Cascadia and SW Japan appear to have a prominent gap in the epicentral distribution of ETS tremors (Figure 9) [*Obara*, 2002; *Obara and Hirose*, 2006]. One difference is that the tremor gap in SW Japan has a lateral dimension of ~70 km, significantly larger than the gap found in mid VI. Another difference is that, according to the Japanese regional earthquake catalog, no large crustal earthquake can be found within the gap zone. The different spatial relationship between the tremor gap and the occurrence of large crustal earthquakes in the two regions might imply that the physical processes responsible for forming a tremor gap are not necessarily the same.

4.3. Depth of ETS Tremors

[52] Although ETS tremor in northern Cascadia tends to reach its peak occurrence in the 25–35 km depth range (Figure 8), it is clear that the distribution is neither along the currently interpreted plate interface nor within a narrow dipping zone. This is at odds with the observations in SW Japan where the majority of nonvolcanic tremors are located in the vicinity (<10 km) of the interpreted interplate thrust zone [e.g., *Ito et al.*, 2007; *Obara and Hirose*, 2006; *Shelly et al.*, 2006, 2007a, 2007b]. This marked difference between these otherwise very similar subduction zones necessitates further verification that our observed depth distribution of tremors is not an artifact of the SSA methodology.

[53] In addition to the arguments presented in previous studies [*Kao et al.*, 2005, 2006, 2007a], we apply the innovative approach of *La Rocca et al.* [2009] to estimate the tremor depths. This approach is based on the following rationale. For each tremor solution, the vertical and the two horizontal component seismograms recorded at the closest broadband station are dominated by *P* wave and *S* wave energy, respectively, if the epicentral distance is small (<15 km). Therefore, the corresponding $S–P$ time can be identified as a prominent peak in the cross correlation function between the vertical component and one of the two horizontal components (depending on the polarity of the *S* wave), imposing a tight constraint on the depth of the tremor source. In Figure 10, we present four representative examples using this new method to demonstrate the existence of ETS tremors at locations other than the interpreted plate interface beneath the northern Cascadia margin [*McCrory et al.*, 2004].

[54] For each case, we mark *S-P* times corresponding to our best solution and a solution fixed at the plate interface. Clearly solutions at shallow depths fit the observed *S-P* peaks much better than deeper solutions. Furthermore, the possibility of having all tremors within a narrow depth range can be ruled out because the observed *S-P* times actually vary by as much as 2 s (corresponding to a depth difference of ~20 km). The reasonable S/N ratios in the presented cases enable us to visually identify *P* and *S* arrivals on seismograms, and thus confirm the shallower depths (Figure 10).

[55] It is important to point out that such determined depths correspond to the locations where both *P* and *S* phases are originated. They can either be the source locations or velocity discontinuities where efficient phase conversion (from *S* to *P* or vice versa) takes place. Given the existence of strong seismic reflectors beneath the northern Cascadia, the possibility of such derived *S-P* times being structure related cannot be completely ruled out. However, because the impedance contrast across these seismic reflectors is in the range of 5–10% [*Hyndman*, 1988; *Spence et al.*, 1985], the amplitude of the converted phase is expected to be much smaller than the original. Since none of the identified *P* or *S* phases in the four cases shown in Figure 10 has a neighboring phase with significantly larger amplitude, the estimated *S-P* times are more likely to represent the depths of the tremor sources than reflectors.

[56] Similar reasoning can also be applied to our tremor solutions obtained from SSA analysis. Because the brightness function depends directly on the waveform amplitudes observed at the predicted arrival times, the brightness of a structure where converted phases are originated would be very small comparing to that of the original source. By always selecting solutions with the maximum brightness during the source-scanning process, the chance of including artifacts from structure-related phases can be avoided.

[57] Examples shown in Figure 10 demonstrate the existence of ETS tremors above the conventionally interpreted plate interface. But we must emphasize that they do not imply all tremors being shallow. In contrary, our results suggest that ETS tremors can occur along the plate interface and even within the subducted oceanic crust (Figure 8). The essence of our analysis is that the peak occurrence of ETS tremors at the depth of the E layer is unlikely to be an error of mislocation.

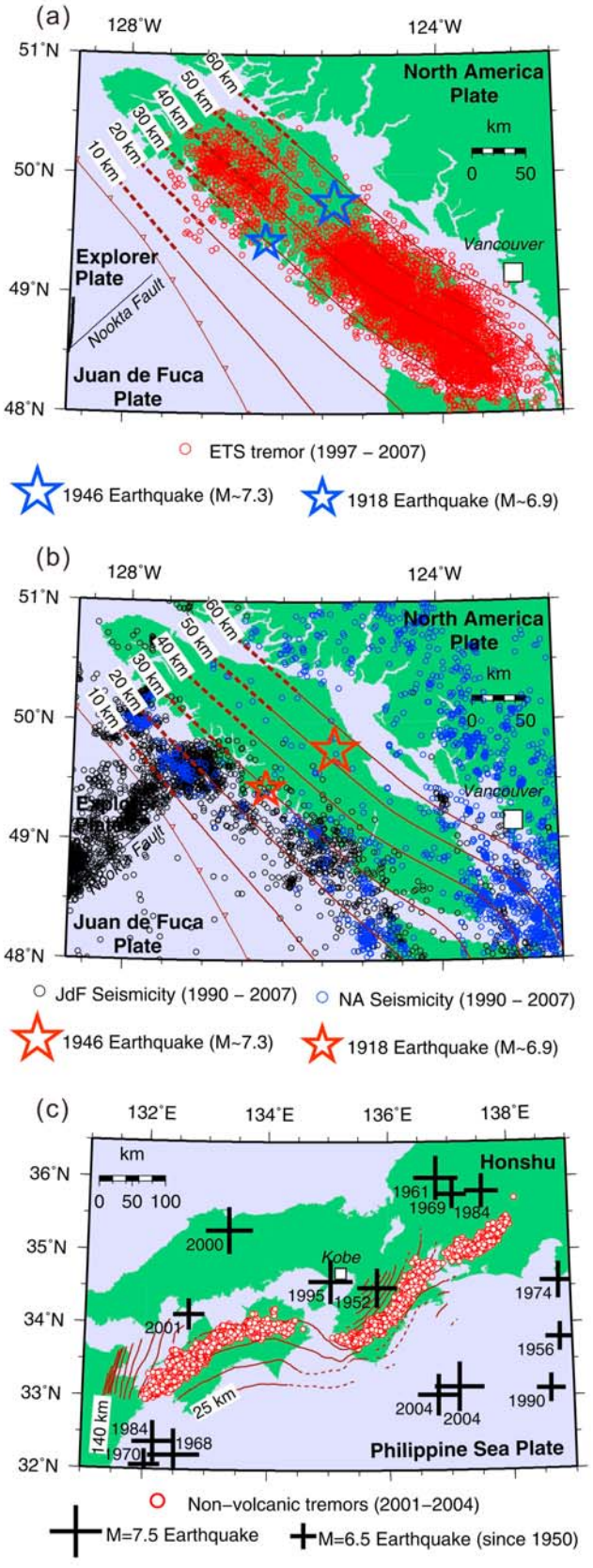

Figure 9. A comparison of ETS tremor distributions and background seismicity in (a and b) northern Cascadia and (c) SW Japan. Tremor catalog and the contour of the plate interface for SW Japan are adapted from *Obara and Hirose* [2006] and *Nakamura et al.* [1997], respectively. Locations of the two large earthquakes in northern Cascadia are discussed in the text, while the epicenters of large ($M > 6.5$) earthquakes in SW Japan are determined by the Japan Meteorological Agency and obtained through the International Seismological Center (online bulletin, Thatcham, United Kingdom, 2001, http://www.isc.ac.uk). Although prominent tremor gaps can be observed for both regions, there are two significant differences, i.e., (1) the northern Cascadia gap corresponds to the epicentral area of large crustal earthquakes in the region and (2) the lateral dimension of the tremor gap in SW Japan is significantly larger.

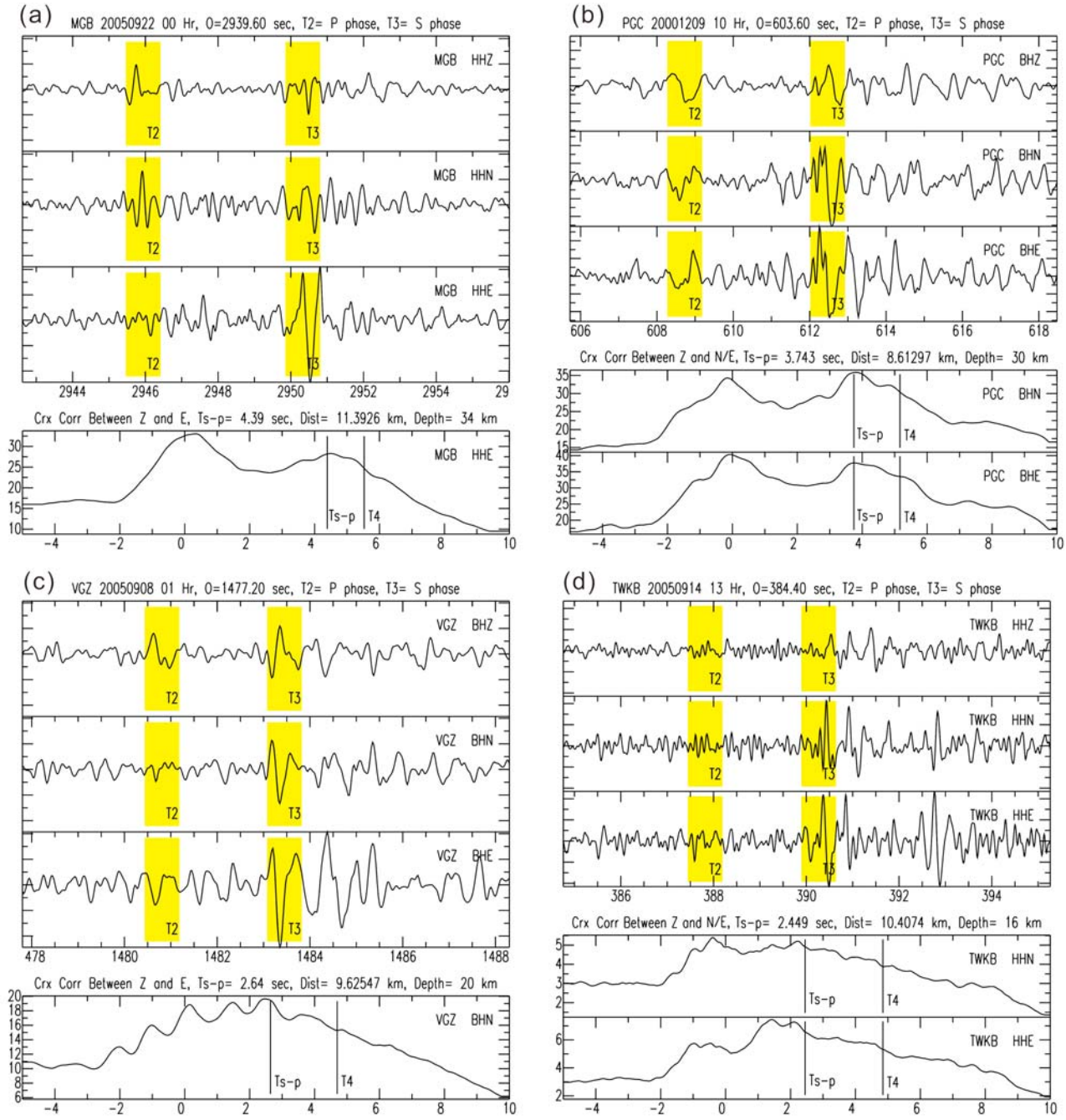

Figure 10. Four examples of ETS tremors at shallow depths above the interpreted interplate thrust zone. For each case, band-pass-filtered three-component seismograms are shown on the top with *P* and *S* phases in highlighting (marked as T2 and T3, respectively), while cross-correlation functions are shown on the bottom. The time difference between *S* and *P* phases for a shallow solution, roughly at the depth of E layer, is marked by Ts-p. T4 marks the corresponding *S-P* time for a solution fixed at the interpreted plate interface ((a) 45, (b) 44, (c) 40, and (d) 41 km). Notice that solutions with shallower depths systematically fit the observation better. Locations of seismic stations are shown in Figure 1.

4.4. ETS Tremors and the E Layer

[58] The spatial correlation between the peak occurrence of tremors and the location of the strong seismic reflectors presents a challenge to the tectonic interpretation and rheological implications of the E layer. This challenge is further complicated by the controversy surrounding the exact location of the plate interface beneath most of VI. The interface has been placed below the E layer based on intraplate seismicity and the location of low-velocity zones from receiver function studies (Figure 8) [e.g., *Cassidy and*

Ellis, 1993; *Fluck et al.*, 1997; *Hyndman*, 1988; *McCrory et al.*, 2004; *Ramachandran et al.*, 2005], at the bottom of the E layer [*Nedimovic et al.*, 2003], and at the top of the E layer [*Nicholson et al.*, 2005]. Recently, an even more complex scenario has been proposed that splits the interface into two shear zones both above and below the E layer [*Calvert*, 2004; *Calvert et al.*, 2006]. Unlike other subduction zones where the plate interface can be located by the frequent occurrence of earthquakes with low-angle thrust faulting, the interplate thrust zone beneath northern Cascadia is largely aseismic and therefore lacks constraints from earthquake focal mechanisms [*Rogers and Horner*, 1991; *Taber and Smith*, 1985].

[59] The distribution of tremors can also be viewed in the context of structural controls, similar to earthquakes. When the distribution of earthquake hypocenters appears to follow a particular geometry, the cluster is usually interpreted as the result of shear dislocation along a specific structure (i.e., fault or fault zone). If the hypocenters tend to scatter within a volume, they are often regarded as the result of strain release in response to the overall elastic deformation. Each individual event, in this case, simply means that the local rheological condition favors seismogenesis, but is not necessarily related to a well-developed fault. Following this analogy, the concentration of tremors in the vicinity of the E layer could be interpreted as the result of structure-controlled shear dislocation, while the more scattered bursts manifest the strain-releasing process in places where local conditions promote tremors.

[60] We speculate that a significant portion of the tremor activity and associated distributed shear displacements may be taking place along well-developed structures such as the E layer, while fewer, perhaps also more random, tremor bursts are generated elsewhere in response to the induced stress variation throughout the volume. When the slip event propagates along the strike of the Cascadia margin, the cluster of tremors would migrate accordingly. Further investigation into the precise depth and distribution of ETS slip, without the a priori assumption that it occurs on any specific structure, is needed to resolve this important issue.

[61] We should mention that deep seismic surveys with clear crustal images down to 60 km depth have been conducted recently in the Shikoku area, SW Japan [*Ito et al.*, 2006; *Sato et al.*, 2005]. While the velocity structure in the overriding crust is very complex, extensive zones of strong seismic reflectors that resemble the E layer beneath northern Cascadia are not observed. If the depth distribution of ETS tremors beneath northern Cascadia implies a more diffused source zone that includes many well-developed structures, then the simpler configuration of the plate interface beneath SW Japan could result in a simpler scenario for the generation of slip and tremor at depth. This perhaps can explain, at least in part, the dramatic difference in the observed depth distribution of tremors between northern Cascadia and SW Japan.

4.5. ETS Recurrence in North Cascadia

[62] Our results can shed some light on the nature of ETS recurrence in northern Cascadia. Although ETS is repeatedly observed in all three sections of VI, from a statistical point of view only the southern section appears to have regular recurrence. The reason for such a remarkable regularity beneath southern VI is not yet clear. Given that no definitive recurrence pattern can be established for the middle or northern sections and assuming no structural differences exist, an alternative explanation may be that the recurrence of ETS is a time-variant process and the regular interval observed in southern VI is only temporary. This would be analogous to the recurrence pattern of characteristic earthquakes along the San Andreas Fault near Parkfield, California, where a regular interval is often but not always observed [e.g., *Bakun and McEvilly*, 1984; *Nadeau and Johnson*, 1998; *Savage*, 1993]. Long-term continuous monitoring of ETS with improved resolution is required to address this question.

5. Conclusions

[63] An ETS scale system is proposed to quantitatively characterize the spatial-temporal sizes of ETS events (Table 1). An episode is categorized as A class if the corresponding lateral dimension (i.e., the length projected onto the strike of the margin) is $\geq$300 km. Lower classes (i.e., B, C, and D) correspond to shorter lateral dimensions (150–300 km, 50–150 km, and <50 km, respectively). The number of weeks is used to categorize the time duration of an ETS episode (0 being less than 3 days; 1, 2, or 3, for up to 1, 2, or 3 weeks, respectively). The number 4 is assigned to episodes longer than 3 weeks.

[64] There is a remarkable correlation between GPS and seismic signatures of major ETS episodes (A or B classes) beneath VI. However, the GPS signature is unclear for most minor episodes. Regular recurrence is only observed for A or B class episodes beneath southern VI (recurrence interval: 447 ± 43 days). No regular recurrence can be confidently determined for the middle and northern sections of VI.

[65] Halting and jumping are very common in ETS migration patterns. Along-strike migration can happen in both directions, but episodes migrating toward the north seem to outnumber those toward the south by ~30%. The daily migration speeds, likely physically meaningful for only A or B class events, can vary significantly even within the same episode, with the average being ~9 km per day. The migration speed does not appear to be affected by the direction of migration.

[66] A prominent tremor gap is found at the boundary between the middle and northern sections of VI around 49.5°N. This gap coincides with the epicenters of the only two large earthquakes (1918, $M \sim 6.9$; 1946 $M \sim 7.3$) beneath VI in the past 150 years. To the south of this gap, the surface projection of ETS tremors closely follows the geometry of the subducted Juan de Fuca plate, and is bounded approximately by the 30 and 50 km depth contours of the interpreted plate interface. The distribution shifts seaward to the north of the gap where the younger Explorer plate is subducting beneath the North America plate at a slower rate.

[67] In general, tremors tend to occur in places where the local seismicity is relatively sparse. One possible explanation for such anticorrelation is that both ETS tremors and ordinary earthquakes are both manifestations of stress release in the crust. The mechanical/rheological conditions in places where fluids are abundant would favor the occurrence of tremors in response to very small stress

changes, thereby preventing the stress accumulations required to generate ordinary earthquakes. Following this logic, the observed tremor gap could imply that mid VI lacks these pliant conditions and stress is accumulating toward the next large crustal earthquake. Alternatively, the tremor gap can be interpreted as a temporal phenomenon due to the modulation of crustal stress by the occurrence of large earthquakes.

[68] The depth distribution of ETS tremors has a peak at the 25–35 km range where strong seismic reflectors (i.e., the E layer) are located. Independent constraints from *S-P* times confirm the existence of tremors in the vicinity of the E-layer. By taking an analogy between tremors and earthquakes, we speculate that a significant portion of the tremor activity and some accompanying crustal shear are probably taking place along well-developed structures such as the E layer, while fewer (and perhaps more random) tremor bursts are generated elsewhere in response to the induced stress variation throughout the source volume. Further investigation into the precise depth and distribution of ETS slip, without the a priori assumption that it occurs on any specific structure, is needed.

[69] **Acknowledgments.** Critical reviews by R. Currie (internal), H. Hirose (Associate Editor), S. Malone, and K. Obara are greatly appreciated. We benefited from discussion with G. Beroza, M. Bostock, M. Brudzinski, K. Creager, R. Hyndman, Y. Ito, T. Melbourne, S. Peacock, J. Rubinstein, D. Shelly, J. Vidale, and K. Wang. Waveform data for the SSA experiment (SW Japan) were kindly provided by NIED, Japan. G. Beroza and D. Shelly provided the velocity model for SW Japan. H. Hirose provided the tremor catalog and the interface contours used in Figure 9. Operation of the BC POLARIS array is supported by the POLARIS consortium. SAC and GMT software packages are used in data processing and plotting, respectively. Most SSA computation was done on the Mercury cluster of the University of Victoria. This research was supported in part by USGS NEHRP research grants 04HQGR0093, 06HQGR0151, and 08HQGR0088. Geological Survey of Canada ESS contribution 20080279.

References

Bakun, W. H., and T. V. McEvilly (1984), Recurrence models and Parkfield, California, earthquakes, *J. Geophys. Res.*, *89*, 3051–3058, doi:10.1029/JB089iB05p03051.

Blais-Stevens, A., G. C. Rogers, and J. J. Clague (2009), A 4000 year record of earthquakes in the late holocene sediments from Saanich Inlet, an anoxic fiord near Victoria, British Columbia, *Seismol. Res. Lett.*, *80*, 294.

Braunmiller, J., and J. Nábelek (2002), Seismotectonics of the Explorer region, *J. Geophys. Res.*, *107*(B10), 2208, doi:10.1029/2001JB000220.

Brudzinski, M. R., and R. M. Allen (2007), Segmentation in episodic tremor and slip all along Cascadia, *Geology*, *35*, 907–910, doi:10.1130/G23740A.1.

Calvert, A. J. (2004), Seismic reflection imaging of two megathrust shear zones in the northern Cascadia subduction zone, *Nature*, *428*, 163–167, doi:10.1038/nature02372.

Calvert, A. J., K. Ramachandran, H. Kao, and M. A. Fisher (2006), Local thickening of the Cascadia forearc crust and the origin of seismic reflectors in the uppermost mantle, *Tectonophysics*, *420*, 175–188, doi:10.1016/j.tecto.2006.01.021.

Cassidy, J. F., and R. M. Ellis (1993), *S* wave velocity structure of the northern Cascadia subduction zone, *J. Geophys. Res.*, *98*, 4407–4421, doi:10.1029/92JB02696.

Cassidy, J. F., R. M. Ellis, and G. C. Rogers (1988), The 1918 and 1957 Vancouver Island earthquakes, *Bull. Seismol. Soc. Am.*, *78*, 617–635.

Cassidy, J. F., R. M. Ellis, C. Karavas, and G. C. Rogers (1998), The northern limit of the subducted Juan de Fuca plate system, *J. Geophys. Res.*, *103*, 26,949–26,961, doi:10.1029/98JB02140.

Chen, W.-P., and M. R. Brudzinski (2007), Repeating earthquakes, episodic tremor and slip: Emerging patterns in complex earthquake cycles, *Complexity*, *12*, 33–43, doi:10.1002/cplx.20185.

Clowes, R. M., M. T. Brandon, A. G. Green, C. J. Yorath, A. S. Brown, E. R. Kanasewich, and C. Spencer (1987), LITHOPROBE-southern Vancouver Island: Cenozoic subduction complex imaged by deep seismic reflections, *Can. J. Earth Sci.*, *24*, 31–51.

Dragert, H., K. Wang, and T. S. James (2001), A silent slip event on the deeper Cascadia subduction interface, *Science*, *292*, 1525–1528, doi:10.1126/science.1060152.

Dragert, H., K. Wang, and G. Rogers (2004), Geodetic and seismic signatures of episodic tremor and slip in the northern Cascadia subduction zone, *Earth Planets Space*, *56*, 1143–1150.

Fluck, P., R. D. Hyndaman, and K. Wang (1997), Three-dimensional dislocation model for great earthquakes of the Cascadia subduction zone, *J. Geophys. Res.*, *102*, 20,539–20,550, doi:10.1029/97JB01642.

Gallego, A., R. M. Russo, D. Compte, V. I. Macanu, R. E. Murdie, and J. C. VanDecar (2007), Non-volcanic seismic tremor in the Chile triple junction region: Active subducted transform faults?, *Eos Trans. AGU*, *88*(23), Jt. Assem. Suppl., Abstract S33A–05.

Hasegawa, H.S., and G.C. Rogers (1978), Quantification of the magnitude 7.3, British Columbia earthquake of June 23, 1946, *Tectonophysics*, *49*, 185–188, doi:10.1016/0040-1951(78)90176-2.

Hirose, H., and K. Obara (2005), Repeating short- and long-term slow slip events with deep tremor activity around the Bungo channel region, southwest Japan, *Earth Planets Space*, *57*, 961–972.

Hirose, H., H. Kao, and K. Obara (2006), Comparative study of non-volcanic tremor locations in the Cascadia subduction zone using two different methods, *Eos Trans. AGU*, *87*(52), Fall Meet. Suppl., Abstract T41A–1533.

Hodgson, E. A. (1946), British Columbia earthquake, June 23, 1946, *J. R. Astron. Soc. Can.*, *40*, 285–319.

Hyndman, R. D. (1988), Dipping seismic reflectors, electrically conductive zones, and trapped water in the crust over a subducting plate, *J. Geophys. Res.*, *93*, 13,391–13,405, doi:10.1029/JB093iB11p13391.

Hyndman, R. D., S. Mazzotti, D. Weichert, and G. C. Rogers (2003), Frequency of large crustal earthquakes in Puget Sound-Southern Georgia Strait predicted from geodetic and geological deformation rates, *J. Geophys. Res.*, *108*(B1), 2033, doi:10.1029/2001JB001710.

Ito, K., Y. Umeda, H. Sato, I. Hirose, N. Hirata, T. Kawanaka, and T. Ikawa (2006), Deep seismic surveys in the Kinki district, Shingu-Maizura line, *Bull. Earthquake Res. Inst. Univ. Tokyo*, *81*, 239–245.

Ito, Y., K. Obara, K. Shiomi, S. Sekine, and H. Hirose (2007), Slow earthquakes coincident with episodic tremors and slow slip events, *Science*, *315*, 503–506, doi:10.1126/science.1134454.

Kao, H., and S.-J. Shan (2004), The source-scanning algorithm: Mapping the distribution of seismic sources in time and space, *Geophys. J. Int.*, *157*, 589–594, doi:10.1111/j.1365-246X.2004.02276.x.

Kao, H., and S.-J. Shan (2007), Rapid identification of earthquake rupture plane using source-scanning algorithm, *Geophys. J. Int.*, *168*, 1011–1020, doi:10.1111/j.1365-246X.2006.03271.x.

Kao, H., S.-J. Shan, H. Dragert, G. Rogers, J. F. Cassidy, and K. Ramachandran (2005), A wide depth distribution of seismic tremors along the northern Cascadia margin, *Nature*, *436*, 841–844, doi:10.1038/nature03903.

Kao, H., S.-J. Shan, H. Dragert, G. Rogers, J. F. Cassidy, K. Wang, T. James, and K. Ramachandran (2006), Spatial-temporal patterns of seismic tremors in northern Cascadia, *J. Geophys. Res.*, *111*, B03309, doi:10.1029/2005JB003727.

Kao, H., S.-J. Shan, G. Rogers, and H. Dragert (2007a), Migration characteristics of seismic tremors in the northern Cascadia margin, *Geophys. Res. Lett.*, *34*, L03304, doi:10.1029/2006GL028430.

Kao, H., P. J. Thompson, G. Rogers, H. Dragert, and G. Spence (2007b), Automatic detection and characterization of seismic tremors in northern Cascadia, *Geophys. Res. Lett.*, *34*, L16313, doi:10.1029/2007GL030822.

Kao, H., P. J. Thompson, S.-J. Shan, G. Rogers, H. Dragert, and G. Spence (2008), Tremor Activity Monitoring System (TAMS) operating in northern Cascadia, *Eos Trans. AGU*, *89*(42), 405–406, doi:10.1029/2008EO420001.

La Rocca, M., K. C. Creager, D. Galluzzo, S. Malone, J. E. Vidale, J. R. Sweet, and A. G. Wech (2009), Cascadia tremor located near plate interface constrained by *S* minus *P* wave times, *Science*, *323*, 620–623, doi:10.1126/science.1167112.

McCausland, W., S. Malone, and D. Johnson (2005), Temporal and spatial occurrence of deep non-volcanic tremor: From Washington to northern California, *Geophys. Res. Lett.*, *32*, L24311, doi:10.1029/2005GL024349.

McCrory, P. A., J. L. Blair, D. H. Oppenheimer, and S. R. Walter (2004), Depth to the Juan de Fuca slab beneath the Cascadia subduction margin: A 3-D model for sorting earthquakes [CD-Rom], *U.S. Geol. Surv. Data Ser.*, 91.

Melbourne, T. I., W. M. Szeliga, M. M. Miller, and V. M. Santillan (2005), Extent and duration of the 2003 Cascadia slow earthquake, *Geophys. Res. Lett.*, *32*, L04301, doi:10.1029/2004GL021790.

Miller, M. M., T. Melbourne, D. J. Johnson, and W. Q. Sumner (2002), Periodic slow earthquakes from the Cascadia subduction zone, *Science*, *295*, 2423, doi:10.1126/science.1071193.

Mooney, W. D., G. Laske, and T. G. Masters (1998), CRUST 5.1: A global crustal model at 5° × 5°, *J. Geophys. Res.*, *103*, 727–747, doi:10.1029/97JB02122.

Nadeau, R. M., and L. R. Johnson (1998), Seismological studies at Parkfield VI: Moment release rates and estimates of source parameters for small repeating earthquakes, *Bull. Seismol. Soc. Am.*, *88*, 790–814.

Nakamura, M., H. Watanabe, T. Konomi, S. Kimura, and K. Miura (1997), Characteristic activities of subcrustal earthquakes along the outer zone of southwestern Japan (in Japanese with English abstract), *Annu. Disaster Prev. Res. Inst. Kyoto Univ.*, *40*, 1–20.

Nedimovic, M. R., R. D. Hyndman, K. Ramachandran, and G. D. Spence (2003), Reflection signature of seismic and aseismic slip on the northern Cascadia subduction interface, *Nature*, *424*, 416–420, doi:10.1038/nature01840.

Nicholson, T., M. Bostock, and J. F. Cassidy (2005), New constraints on subduction zone structure in northern Cascadia, *Geophys. J. Int.*, *161*, 849–859, doi:10.1111/j.1365-246X.2005.02605.x.

Obara, K. (2002), Nonvolcanic deep tremor associated with subduction in southwest Japan, *Science*, *296*, 1679–1681, doi:10.1126/science.1070378.

Obara, K., and H. Hirose (2006), Non-volcanic deep low-frequency tremors accompanying slow slips in the southwest Japan subduction zone, *Tectonophysics*, *417*, 33–51, doi:10.1016/j.tecto.2005.04.013.

Obara, K., K. Kasahara, S. Hori, and Y. Okada (2005), A densely distributed high-sensitivity seismograph network in Japan: Hi-net by National Research Institute for Earth Science and Disaster Prevention, *Rev. Sci. Instrum.*, *76*, 021301.1–021301.12, doi:10.1063/1.1854197.

Page, R. (1968), Focal depths of aftershocks, *J. Geophys. Res.*, *73*, 3897–3903, doi:10.1029/JB073i012p03897.

Peacock, S. M. (1990), Fluid processes in subduction zones, *Science*, *248*, 329–337, doi:10.1126/science.248.4953.329.

Ramachandran, K., S. E. Dosso, G. D. Spence, R. D. Hyndman, and T. M. Brocher (2005), Forearc structure beneath southwestern British Columbia: A three-dimensional tomographic velocity model, *J. Geophys. Res.*, *110*, B02303, doi:10.1029/2004JB003258.

Rogers, G., and H. Dragert (2003), Episodic tremor and slip on the Cascadia subduction zone: The chatter of silent slip, *Science*, *300*, 1942–1943, doi:10.1126/science.1084783.

Rogers, G. C. (1983), Seismotectonics of British Columbia, Ph.D. thesis, Univ. of B. C., Vancouver, B. C., Canada.

Rogers, G. C., and H. S. Hasegawa (1978), A second look at the British Columbia earthquake of June 23, 1946, *Bull. Seismol. Soc. Am.*, *68*, 653–675.

Rogers, G. C., and R. B. Horner (1991), An overview of western Canadian seismicity, in *Neotectonics of North America*, edited by D. B. Slemmons et al., pp. 69–76, Geol. Soc. Am., Boulder, Colo.

Sato, H., et al. (2005), Crustal structure of the outer zone in southwest Japan revealed by Shikoku and Seto-Inland-Sea seismic profiling in 2002, *Bull. Earthquake Res. Inst. Univ. Tokyo*, *80*, 53–71.

Savage, J. C. (1993), The Parkfield prediction fallacy, *Bull. Seismol. Soc. Am.*, *83*, 1–6.

Schwartz, S. Y., and J. M. Rokosky (2007), Slow slip events and seismic tremor at circum-pacific subduction zones, *Rev. Geophys.*, *45*, RG3004, doi:10.1029/2006RG000208.

Shelly, D. R., G. C. Beroza, S. Ide, and S. Nakamula (2006), Low-frequency earthquakes in Shikoku, Japan, and their relationship to episodic tremor and slip, *Nature*, *442*, 188–191, doi:10.1038/nature04931.

Shelly, D. R., G. C. Beroza, and S. Ide (2007a), Non-volcanic tremor and low-frequency earthquake swarms, *Nature*, *446*, 305–307, doi:10.1038/nature05666.

Shelly, D. R., G. C. Beroza, and S. Ide (2007b), Complex evolution of transient slip derived from precise tremor locations in western Shikoku, Japan, *Geochem. Geophys. Geosyst.*, *8*, Q10014, doi:10.1029/2007GC001640.

Spence, G. D., R. M. Clowes, and R. M. Ellis (1985), Seismic structure across the active subduction zone of western Canada, *J. Geophys. Res.*, *90*, 6754–6772, doi:10.1029/JB090iB08p06754.

Szeliga, W., T. Melbourne, M. Santillan, and M. Miller (2008), GPS constraints on 34 slow slip events within the Cascadia subduction zone, 1997–2005, *J. Geophys. Res.*, *113*, B04404, doi:10.1029/2007JB004948.

Taber, J. J., and S. W. Smith (1985), Seismicity and focal mechanisms associated with the subduction of the Juan de Fuca plate beneath the Olympic Peninsula, Washington, *Bull. Seismol. Soc. Am.*, *75*, 237–249.

Wang, K., H. Dragert, H. Kao, and E. Roeloffs (2008), Characterizing an "uncharacteristic" ETS event in northern Cascadia, *Geophys. Res. Lett.*, *35*, L15303, doi:10.1029/2008GL034415.

H. Dragert, H. Kao, G. Rogers, and S.-J. Shan, Geological Survey of Canada, Natural Resources Canada, Pacific Geoscience Centre, P.O. Box 6000, Sidney, BC V8L 4B2, Canada. (hkao@nrcan.gc.ca)